UNIVERSIDADE FEDERAL DE MINAS GERAIS
ESCOLA DE ENGENHARIA
PROGRAMA DE PÓS-GRADUAÇÃO EM ENGENHARIA DE ESTRUTURAS

Bruna Luiza Nolli

POST-BUCKLING ANALYSIS OF METAL AND COMPOSITE REINFORCED PANELS

Belo Horizonte
2019

Bruna Luiza Nolli

POST-BUCKLING ANALYSIS OF METAL AND COMPOSITE REINFORCED PANELS

Dissertação apresentada ao Programa de Pós-Graduação em Engenharia de Estruturas da Universidade Federal de Minas Gerais requisito parcial para obtenção do título de Mestre (a) em Engenharia de Estruturas.

Orientador: Carlos Alberto Cimini

Belo Horizonte
2019

Nolli, Bruna Luiza.
N796p Post-buckling analysis of metal and composite reinforced panels [recurso eletrônico] /Bruna Luiza Nolli. - 2019.
1 recurso online (x, 67 f. : il., color.) : pdf.

Orientador: Carlos Alberto Cimini Júnior.

Dissertação (mestrado) - Universidade Federal de Minas Gerais, Escola de Engenharia.

Apêndice: f.65-67.
Bibliografia: f.63-64.

Exigências do sistema: Adobe Acrobat Reader.

1. Engenharia de Estruturas - Teses. 2. Flambagem (Mecânica) - Teses. 3. Modelo de métodos finitos - Teses. 4. Materiais compostos – Teses. I. Cimini Júnior, Carlos Alberto. II. Universidade Federal de Minas Gerais. Escola de Engenharia. III. Título.

CDU: 624(043)

Ficha catalográfica: Biblioteca Profº Mário Werneck, Escola de Engenharia da UFMG

PROPEEs

UNIVERSIDADE FEDERAL DE MINAS GERAIS
Programa de Pós-Graduação em Engenharia de Estruturas

UFMG

ATA DA DEFESA DE DISSERTAÇÃO DE MESTRADO EM ENGENHARIA DE ESTRUTURAS Nº: **357** da aluna **Bruna Luiza Nolli.**

Às **15h** horas do dia **17** do mês de **junho** de **2019**, reuniu-se, na Escola de Engenharia da Universidade Federal de Minas Gerais - UFMG, a Comissão Examinadora indicada pelo Colegiado do Programa, incluindo o convidado Ms. Cristiano Alves Pena da Embraer em **30 de maio de 2019**, para julgar a defesa da Dissertação de Mestrado intitulada **"Post-Buckling Analysis of Metal and Composite Reinforced Panels"**, cuja aprovação é um dos requisitos para a obtenção do Grau de MESTRE EM ENGENHARIA DE ESTRUTURAS na área de .

Abrindo a sessão, o Presidente da Comissão, **Prof. Dr. Carlos Alberto Cimini Jr.**, após dar a conhecer aos presentes o teor das Normas Regulamentares passou a palavra à candidata para apresentação de seu trabalho. Seguiu-se a arguição pelos examinadores, com a respectiva defesa da candidata. Logo após, a Comissão se reuniu, sem a presença da candidata e do público, para julgamento e expedição do resultado final. Foram atribuídas as seguintes indicações:

(Aprov./Repr.)

Prof. Dr. Carlos Alberto Cimini Jr. - DEES - UFMG (Orientador) APROVADA
Prof. Dr. Marcelo Greco - DEES-UFMG APROVADA
Dra. Cristina Ferreira de Paula - EMBRAER APROVADA

Pelas indicações acima, a candidata foi considerada APROVADA, conforme pareceres em anexo.

O resultado final foi comunicado publicamente à candidata pelo Presidente da Comissão.

Nada mais havendo a tratar, o Presidente encerrou a reunião e lavrou a presente ATA, que será assinada por todos os membros participantes da Comissão Examinadora. Belo Horizonte, 17 de junho de 2019.

Carlos Alberto Cimini Jr.
Marcelo Greco
Cristina Ferreira de Paula

Observações:

1) A aprovação da candidata na defesa da Dissertação de Mestrado não significa que a mesma tenha cumprido todos os requisitos necessários para obtenção do Grau de Mestre em Engenharia de Estruturas;
2) Este documento não terá validade sem a assinatura e carimbo do Coordenador do Programa de Pós-Graduação.

ACKONOWLEDGMENT

I am profoundly grateful to my parents, that taught me to dedicate 100% of my efforts in everything I decided to do, so that in the end there would be no regrets with the achieved results. To my brother that showed me life is too short not to take risks, even if it is just a little. And to my husband, for all the help, care and patience during all the years that I have dedicated to my master's degree, and for all the encouragements every time I thought in giving up. Thank you.

Take the first step in faith.

You don't have to see the whole staircase, just take the first step.

Martin Luther King Jr

RESUMO

A indústria aeronáutica tem como objetivo aumentar a eficiência e reduzir os custos de suas aeronaves, a fim de desenvolver aviões com melhor desempenho e menor consumo de combustível. As pesquisas demonstraram que os painéis de cisalhamento podem suportar uma quantidade significativa de carga após atingir sua carga inicial de flambagem. Portanto, explorar a capacidade pós-flambagem de painéis reforçados em materiais compósitos resulta em estruturas mais leves e menos dispendiosas.

Para os painéis reforçados metálicos existe uma metodologia consolidada para o cálculo de tração diagonal desenvolvida pela NASA (National Aeronautics and Space Administration), NACA TN2661 (Kuhn, Peterson e Levin, 1952a). Todavia, para os painéis reforçados em material compósito não existe um método e sim estudos, que em sua maioria estão tentando adaptar o método NACA TN2661 para materiais compósitos, levando em consideração a anisotropia do material. Mas esses estudos não consideram o fato de que a anisotropia não é a única característica do material que afeta o comportamento pós-flambagem. A sequência de empilhamento e a orientação das fibras têm influência na análise de flambagem, portanto, elas têm efeitos no comportamento pós-flambagem.

Dessa forma, este estudo foi desenvolvido para aprimorar a compreensão do comportamento pós-flambagem em painéis reforçados em compósitos, e construir um modelo de elementos finitos a ser utilizado em projetos futuros de análise de tração diagonal em painéis reforçados, reduzindo as despesas com testes. Os principais objetivos deste estudo são desenvolver um método para calibrar um modelo de elementos finitos para representar o comportamento de pós-flambagem do painel reforçado em compósito evitando o uso de resultados experimentais; estudar as variações na sequência de empilhamento de painéis reforçados em compósito na análise pós-flambagem; escolha do painel reforçado que tem o melhor comportamento durante a análise pós-flambagem: metálico ou compósito.

Os resultados mostraram que o modelo de elementos finitos desenvolvido neste estudo, considerando a carga, as condições de contorno e os materiais descritos, representa o comportamento do painel reforçado em compósito e seu comportamento na pós-flambagem. Além disso, após a comparação entre seis modelos de painéis reforçados em compósitos com diferentes sequências de empilhamento, o empilhamento que apresentou os menores valores

para os índices de falha foi o de + 45º e-45º nas camadas externas. Este laminado foi escolhido para ser comparado com o modelo do painel reforçado metálico, e esta comparação mostrou que o painel reforçado em compósito suporta cargas mais elevadas. Assim, o painel reforçado em compósito é considerado o melhor para a análise do comportamento do pós-flambagem.

Palavras-chave: tração diagonal, análise de pós-flambagem, modelo de elementos finitos, material compósito.

ABSTRACT

Aeronautic industry is aiming to increase the efficiency and to reduce the costs of their aircrafts, in order to develop airplanes with better performance and lower fuel consumption. Researches have demonstrated that shear panels can carry a significant amount of load after reaching its initial buckling load. Therefore, exploring the post-buckling capacity of composite materials reinforced panels results in lighter and less expensive structures.

For the metallic reinforced panels there is a consolidated methodology developed by NASA (National Aeronautics and Space Administration) to calculate the diagonal tension, NACA TN2661 (Kuhn, Peterson and Levin, 1952a). For the composite reinforced panels, most studies are trying to adapt this method for composite materials, taking into account the anisotropy of the material. But they do not consider the fact that anisotropy is not the only characteristic of the material that affects the post-buckling behavior. Stacking sequence, and fibers orientation have influence in buckling analysis, therefore they have effects in the post-buckling behavior.

Therefore, this study was developed to improve the understanding of the post-buckling behavior in composite reinforced panels, and to build a finite element model to be used in reinforced panel design, reducing the expenses with tests. The main goals of this study are to develop a method to calibrate a FEM to represents the post-buckling behavior of the composite reinforced panel without having to use experimental results; study the variations in stacking sequence in post-buckling analysis; choose the reinforced panel that have the best behavior during the post-buckling analysis: metallic or composite.

The results have shown that the FEM developed in this study, considering the load, boundary conditions and materials described, can represent the behavior of the composite reinforced panel and its post-buckling behavior. Also, after the comparison between six composite reinforced panels models with different stacking sequence, the layup that presented the lowest values for the failure indices was the one with +45 and -45 at the outside layers. This laminate was chosen to be compared with the metallic reinforced panel model, and this comparison have shown that the composite reinforced panel could withstand higher loads, so it is considered the best for the post-buckling behavior analysis.

Keywords: Diagonal Tension, Post-Buckling Analysis, Finite Element Model, Composite Material

FIGURES LIST

TABLES LIST

SIMBOLS LIST

f_c	Compression stress
f_t	Tension stress
P	Load acting in the reinforced panel
q	Shear flow
k	Diagonal tension factor
f_S	Total shear in the web
f_{SR}	Shear stress
f_{DT}	Stress carried by the diagonal tension
mm	Millimeters
t_u	Vertical stiffeners thickness
t	Panel's web thickness
d	Distance between fasteners of vertical stiffeners
h	Panel height
f_{smax}	Maximum stress in the middle of panel
C_1	Angle factor
C_2	Stress concentration factor
f_s	Shear nominal stress in the web
MPa	Megapascal
N	Newton
h_e	Effective height, measured between horizontal stiffeners centroids
$\frac{f_s}{F_{scr}}$	Loading factor
F_{scr}	Critical shear stress between two stiffeners
K_{ss}	Theoretical buckling coefficient for plates with simple supported edges
d_c	Distance between fasteners of vertical stiffeners

E	Young's modulus
h_c	Beam height between fasteners
α	Angle between the neutral axes of panel's web and the direction of diagonal tension
f_u	Average stress in vertical stiffener
A_{ue}	Horizontal and vertical stiffeners effective area
wd	Flange flexibility factor
E_1, E_2, E_3	Young's modulus along the principal ply directions
G_{12}, G_{23}, G_{13}	Shear modulus in 1-2, 2-3 e 1-3 planes
$\nu_{12}, \nu_{23}, \nu_{13}$	Poisson's ratio
E_m, E_{1f} e E_{2f}	Young's modulus of matrix and fiber in longitudinal and transversal direction, respectively
V_f, V_m e V_v	Volume ratio for fiber, matrix and void;
W_f and W_m	Weight ratio for fiber and matrix;
ν_m and ν_{12f}	Poisson's ratio for matrix and fiber in longitudinal direction;
G_{12f} and G_m	Shear modulus for fiber and matrix
Q_{11}, Q_{22}, Q_{12}, Q_{66}	Reduced stiffnesses in the lamina principal axis
Q_{xx}, Q_{yy}, Q_{xy}, Q_{xs}, Q_{ys}, Q_{ss}	Reduced stiffnesses in the reference stress coordinate system
$\varepsilon_{xu}{}^T$and $\varepsilon_{yu}{}^T$	Ultimate longitudinal tensile and compressive strain, respectively;
$\varepsilon_{xu}{}^C$ and $\varepsilon_{yu}{}^C$	Ultimate transverse tensile and compressive strain, respectively
γ_{xyu}	Ultimate in-plane shear strain
$X^T$and Y^T	Ultimate longitudinal tensile and compressive stress, respectively
X^C and Y^C	Ultimate transverse tensile and compressive stress, respectively
S	Ultimate in-plane shear stress.
$[K]$	Overall stiffness matrix
$[K_a]$	Linear stiffness matrix

$[K_d]$	Differential stiffness matrix
$[U]$	Total potential energy
u_i	Displacement of i-th degree of freedom
P_a	Applied load
P_{cr_i}	Critical buckling load
λ_i	Eigenvalue
E_x, E_y	Young's modulus in the stress coordinate system
Gxy	Shear modulus in the stress coordinate system
νxy and νyx	Poisson's ratio in the stress coordinate system

ABBREVIATIONS AND ACRONYMS LIST

NASA	National Aeronautics and Space Administration
FEM	Finite element model
PDT	Pure Diagonal Tension
SR	Shear Resistant web
PS	Pure Shear
Glare	GLAss REinforced aluminum
COCOMAT	Improved MATerial Exploitation at Safe Design of COmposite Airframe Structures by Accurate Simulation

SUMMARY

1

1 INTRODUCTION

The challenge of aeronautic industry are to save weight and to reduce the costs of their aircrafts through the combination of different materials and calculation methods. Applications of composite materials have grown, consequently, the challenges to find optimal designs and new developments emerged (Arakaki and Faria, 2016). The use of composite materials to build panel's web at wings and fuselage where they are allowed to undergo an elastic buckling (diagonal tension state), is one way to achieve this goal (Jodoin et al., 2002).

It is possible to design thinner web structures made of composite material using the methodology that evaluates the panel post-buckling behavior, comparing it to other methods, resulting in a lighter final product. This improvement in weight is feasible because the diagonal tension method allows the reinforced panel to buckle after a pre-defined load, but this is not the failure of the structure. At this moment, diagonal folds appear in the panel's web, and the shear forces that caused the buckling are resisted by tension in the web by the diagonal folds, and by compression in the stiffeners (Niu, 2005). Therefore, the final structure can be designed to support tension loads, and the tensions allowable are greater than the compressions one, so the complete structure withstand greater loads.

For the metallic reinforced panel there is a consolidated methodology developed by NASA (National Aeronautics and Space Administration) to calculate the panel's diagonal tension, NACA TN2661 (Kuhn, Peterson and Levin, 1952a). This semi-empiric method was developed based in several tests performed with aluminum panels using different geometries and loads and is widely used by aircrafts manufactures. But a theory for the panel's post-buckling behavior in composite reinforced panels is still in development. There are some researches

(Wittenberg, et al., 2001 and Jodoin et al., 2002) trying to adapt the NACA TN-2661 (Kuhn, Peterson and Levin, 1952a) method for composite materials making it account for the anisotropy of the material and corroborate the results with tests. Most of them used GLARE (GLAss REinforced aluminum) to build the panel. Some other studies (Agarwal, 1981, Herrero, 2007 and Melo, 1993) were based in modeling the reinforced panel in finite elements and compared the results with tests data. Yet it was used a one bay panel with unidirectional load.

To improve the understanding of post-buckling behavior in composite reinforced panels, the studies should be focused in the variables that affect this behavior, like stacking sequence, and orientation of the layers. And to overcome the expenses with tests, the reinforced panels modeled in finite element should have more than one bay, vertical and horizontal stiffeners and a complete layup using layer with different orientations. Therefore, the main goals of this study were to develop a method to calibrate a FEM to represents the post-buckling behavior of the composite reinforced panel without having to use experimental results; study the variations in stacking sequence in post-buckling analysis; and choose the reinforced panel that have the best behavior during the post-buckling analysis: metallic or laminate.

The methodology developed in this study consist in five steps described hereafter. The first step was to build a FEM for an aluminum reinforced panel. A linear static analysis, a linear buckling analysis and a non-linear analysis were performed.

The second step was a comparison between results from the hand calculation for diagonal tension using NACA TN2661 (Kuhn, Peterson and Levin, 1952a) method and FEM analysis, in order to guarantee that the model is calibrated. Then a comparison between the buckling loads obtained from the linear and non-linear analyzes was performed.

Step three is a verification of the use of the calibrated mesh to build a FEM for the composite reinforced panel. In order to perform the verification, it was built two models: one with the equivalent properties for the layup chosen, and the other one modeling each layer and using the material properties of the tape. The models result from linear buckling analysis, and from the non-linear analysis, were compared.

Step four consisted in select the stacking sequence and the angle of fiber orientations for the layups. For each layup, a FEM was created modeling each layer and entering the material properties of the tape. Also, for each layup it was applied several different loads at the panel. A non-linear analysis for each model was performed, and the failure index of the step when the

diagonal tension is complete, and the panel's web redistribute the compressive load to the stiffeners for all of them was compared. The layup that presented the lowest values for the failure index for all the loads was chosen to be the laminate having the best behavior for the post-buckling analysis.

The fifth step was to build a metallic reinforced panel FEM with the same weight that the composite reinforced panel layup chosen in step four. Then compare the models results from linear buckling analysis, and from the non-linear analysis, in order to determine, which one has the best behavior for the post-buckling analysis.

2

2 PROBLEM STATEMENT

The methodology developed by NASA to calculated metallic reinforced panel's diagonal tension, NACA TN2661 (Kuhn, Peterson and Levin, 1952a) is a semi-empiric method used by several aircrafts manufactures. But a theory for composite reinforced panel's post-buckling behavior is still under development. There are some researches (Wittenberg, et al., 2001 and Jodoin et al., 2002) trying to adapt the NACA TN-2661 (Kuhn, Peterson and Levin, 1952a) method for composite materials making it account for the anisotropy of the material and corroborate the results with tests. Most of them used GLARE (GLAss REinforced aluminum) to build the panel. Some other studies (Agarwal, 1981, Herrero, 2007 and Melo, 1993) were based in modeling the reinforced panel in finite elements and compared the results with tests data. Yet it was used a one bay panel with unidirectional load.

The first main goal of this study was to develop a method to calibrate a FEM to represents the post-buckling behavior of the composite reinforced panel without having to use experimental results. This would overcome the expenses with tests, also would permit the aircraft manufactures to use the model to design the structures.

The second main goal is to improve the understanding of the effects of the variation in stacking sequence and orientation of the layers at the post-buckling behavior of the composite reinforced panels. To do so it was chosen six different layups, symmetric and balanced, all using the same number of laminae with 0º, 90º, 45º and -45º orientation in different stacking sequence. For each layup, a FEM was created modeling each layer and using the material properties of the tape. Also, for each layup it was applied several different loads values at the panel, in order to evaluate the reinforced panel behavior for different loads magnitude. A non-linear analysis for each model was performed, and the failure index of the step when it first occurs the diagonal

tension for all of them was compared. The layup that presents the lowest values for the failure index for all the loads was chosen to be the laminate having the best post-buckling behavior.

The third main goal was to choose the reinforced panel that have the best behavior during the post-buckling analysis: metallic or composite. Two FEM for the reinforced panels, metallic and composite, were built. Both panels have the same mass, and it results of buckling load and first step that occurs diagonal tension were compared.

3

3 LITERATURE REVIEW

3.1 Diagonal Tension

In 1929 Professor Herbert Wagner proved that the metallic reinforced panels did not fail when they buckled between stiffeners. During tests performed in reinforced panels that only carry shear during buckling, he observed that diagonal folds were formed in the panel's web, which work as tension stripes, and the stiffeners began to work as compression columns. In this configuration, the reinforced panel was capable of carrying more load than the buckling load. Therefore, Wagner proofs that the theories and methods used to calculate structures in shear and compression were conservative, resulting in heavier structures. (Kuhn, 1956).

As mention in Bruhn, 1973, Wagner's theory is based in truss structures, as presented in Figure 3.1. For the load P (lower than the buckling load), members A and B share the shear stress equally, but A suffers compression (f_c) and B tension (f_t).

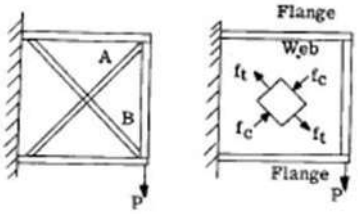

Figure 3.1 – Diagonal Tension in truss (part 1).
Adapted from Bruhn, 1973, p. C11.1.

When the P load reaches the truss buckling load, the member A do not carry any more load. All the shear stress is carried as tension by member B and as compression by the upper and lower stiffeners, as can be seen in Figure 3.2.

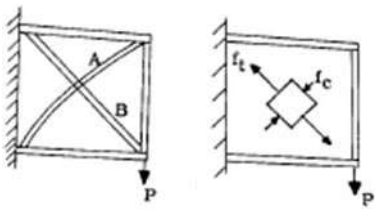

Figure 3.2 – Diagonal Tension in truss (part 2).
Adapted from Bruhn, 1973, p. C11.1.

Niu, 2005 affirms that a panel with thin web presents the same behavior as the truss presented before. The shear stress is carried as tension and compression in ±45° until the buckling of the structure. Figure 3.3 presents the shear flow (q) in a unit element in the middle of panel's web reacting to pure shear.

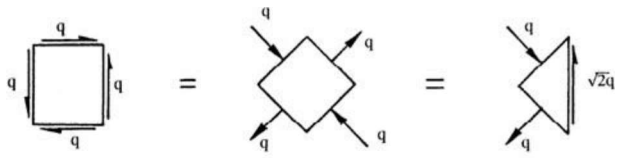

Figure 3.3 – Principal stresses in a web resisting to pure shear.
Niu, 2005, p. 474.

By the time the load P reaches the buckling load, diagonal folds are formed in the panel's web (see Figure 3.4), and they start to behave like the member B shown in Figure 3.2.

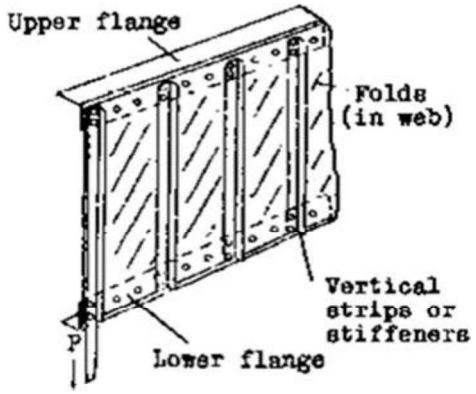

Figure 3.4 – Metallic reinforced panel behavior under shear load.
Wagner, 1928, p. 22.

If it was possible to increase the load P infinitely without the collapse of the structure, the compression load would be so small compared to the tension load that it could be neglected. This idealized scenario is characterized as Pure Diagonal Tension (PDT). In Figure 3.5 it is possible to see the shear flow (q) in a unit element in the middle of panel's webs in PDT.

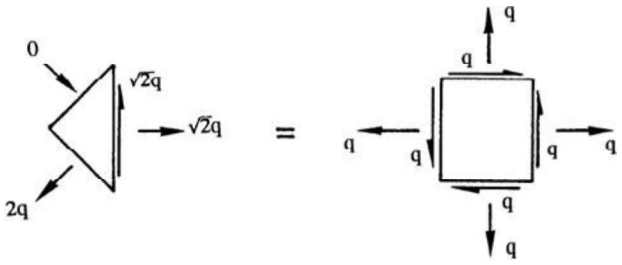

Figure 3.5– Load distribution of a PDT web.
Niu, 2005, p. 483.

According to Kuhn, Peterson and Levin, 1952a, metallic reinforced panels designed for PDT would buckle as soon as any load is applied in the structure. Therefore, it is most common to design structures for the Incomplete Diagonal Tension state, which is a condition between the PDT and the Pure Shear (in which the structure never buckles). In Figure 3.6 it can be seen the stress state for each one of these design conditions.

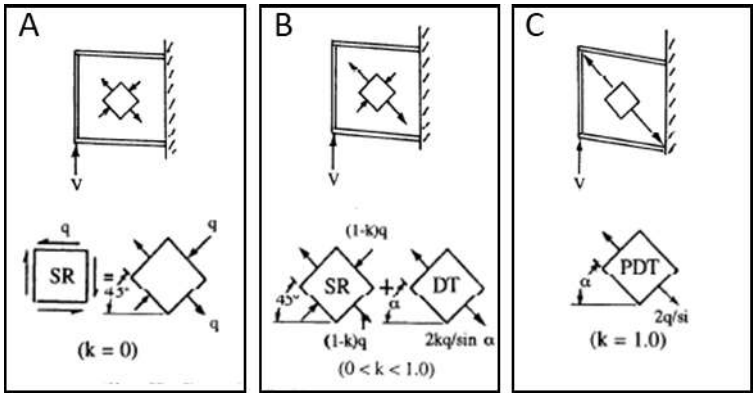

Figure 3.6– Web stresses at different stages of the Diagonal Tension buckled web.
Niu, 2005, p. 484 e 485.

Figure 3.6-A shows the Pure Shear condition (SR - Shear Resistant web), in which the shear stress in reacted as tension and compression in ±45°, there is no buckling and the diagonal tension factor (k) is zero. The Incomplete Diagonal Tension is presented in Figure 3.6-B, in which the panel's web has already buckled. It presents the diagonal folds that support the tension loads, and it is still capable of carrying compressive load. The horizontal stiffeners are in compression and help to carry the remaining compressive load. This is the intermediate condition between PS (Pure Shear) and PDT, and the diagonal tension factor (k) varies from zero to one. In Figure 3.6-C it can be observed the PDT, in which the panel's web carries only tension load, and the horizontal and vertical stiffeners carry the compression. The diagonal tension factor (k) is one.

In the Incomplete Diagonal Tension condition, the total shear in the web (f_S) can be defined as the summation of the shear stress (f_{SR}) and the stress carried by the diagonal tension (f_{DT}) (Niu, 2005). Equations (3.1), (3.2) and (3.3) present this definition.

$$f_S = f_{SR} + f_{DT} \tag{3.1}$$

$$f_{SR} = (1-k) f_S \tag{3.2}$$

$$f_{DT} = k f_S \tag{3.3}$$

3.1.1 NACA TN2661 (Kuhn, Peterson and Levin, 1952a)

According to Bruhn, 1973, NASA (National Aeronautics and Space Administration) developed a program to improve the Diagonal Tension method developed by Wagner. The main goal of the study was to reduce the conservatism and unify the method, in order to apply it in the design of new aircrafts (Kuhn, Peterson and Levin, 1952b).

The semi-empiric method was developed based in 50 testes performed by NASA and 140 tests performed by private companies (Boeing Aircraft Co., Consolidated Aircraft Corp., Douglas Aircraft Co. Inc, The Glenn L. Martin Co. E Vultee Aircraft Corp.). Figure 3.7 shows one of the tests performed.

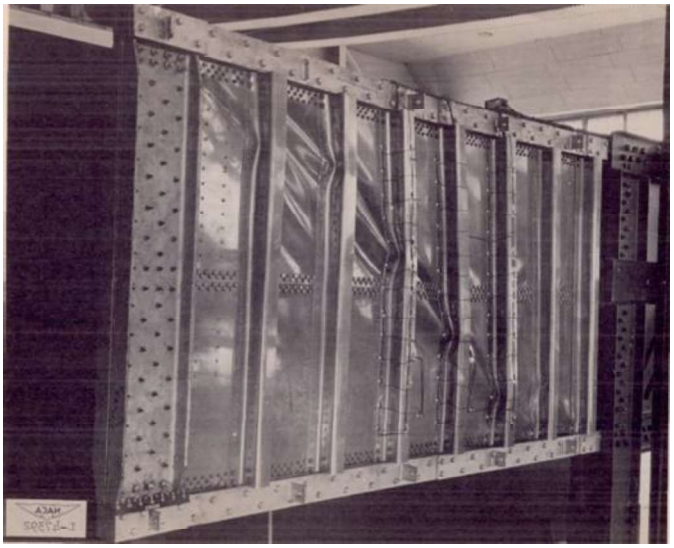

Figure 3.7 – Diagonal Tension: – Experimental Evidences.
Kuhn, Peterson and Levin, 1952b, p. 49.

Despite the greater number of tests, the new method still presents geometric limitation:

a) $\frac{tu}{t} > 0{,}6$
b) $0{,}2 < \frac{d}{h} < 1{,}0$
c) $200 < \frac{h}{t} < 1500$

t_u is the vertical stiffeners thickness [mm], t is panel's web thickness [mm], d is the distance between fasteners of vertical stiffeners [mm] (see Figure 3.8), and h is the panel height [mm] (see Figure 3.8).

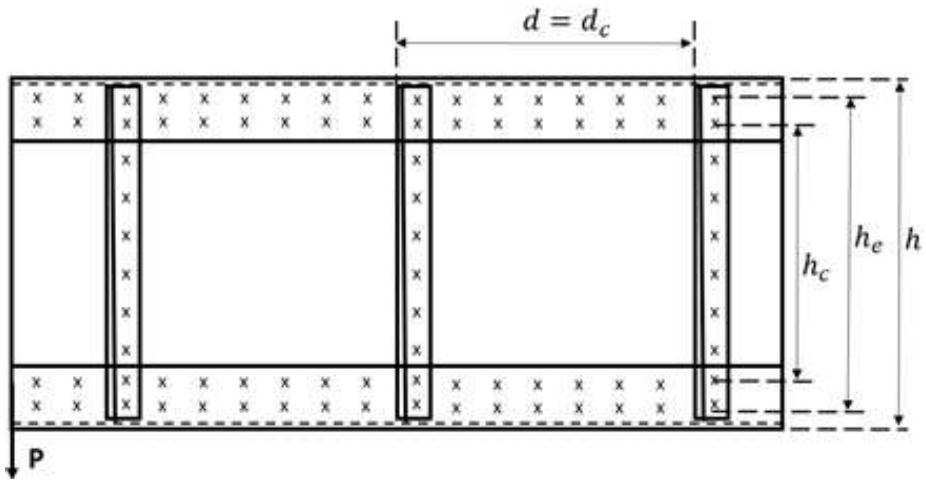

Figure 3.8 – Dimensions and nomenclatures of NACA TN 2661 (Kuhn, Peterson and Levin, 1952a) method.

The maximum stress in the middle of panel (f_{smax}) is described by Eq.(3.4).

$$f_{smax} = f_s(1 + kC_1)(1 + kC_2) \tag{3.4}$$

C_1 is the angle factor, C_2 is the stress concentration factor, and f_s is the shear nominal stress in the web [MPa].

The shear nominal stress in the web f_s is calculated in Eq.(3.5).

$$f_s = \frac{P}{h_e\, t} \tag{3.5}$$

P is the load acting in the panel [N], and h_e is the effective height, measured between horizontal stiffeners centroids [mm] (see Figure 3.9).

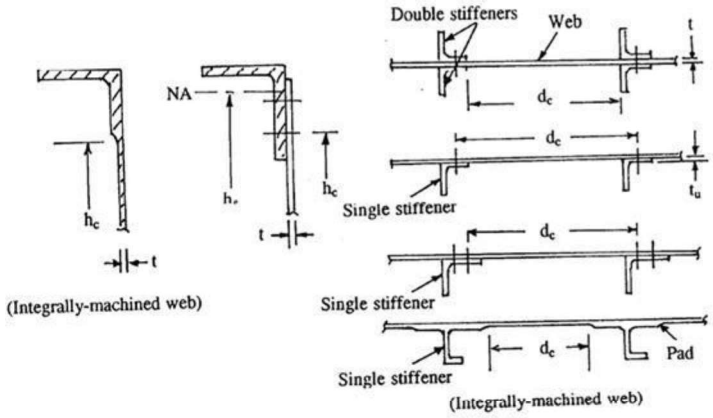

Figure 3.9 - Dimensions and nomenclatures of NACA TN 2661 (Kuhn, Peterson and Levin, 1952a) method. Adapted from Niu, 2005, p. 486.

The diagonal tension factor (k) is obtained in the graph presented in Figure 3.10, in which the loading factor $\frac{fs}{F_{scr}}$ is the input data.

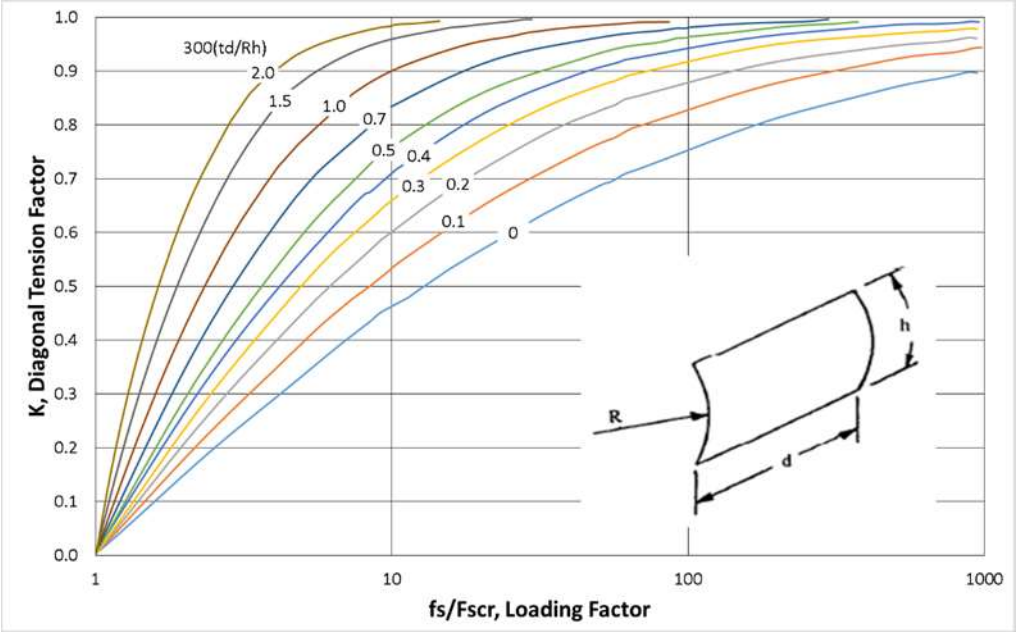

Figure 3.10– Diagonal tension factor (k).
Adapted from Niu, 2005, p. 490.

The critical shear stress between two stiffeners F_{scr} is presented in Eq.(3.6):

$$F_{scr} = K_{ss} E \left(\frac{t}{d_c}\right)^2 \tag{3.6}$$

K_{ss} is the theoretical buckling coefficient for plates with simple supported edges, d_c is the distance between fasteners of vertical stiffeners [mm] (see Figure 3.8), and E is the Young's modulus.

The K_{ss} is reached by the graph presented in Figure 3.11 using the ratio between $\frac{hc}{d_c} = \frac{a}{b}$ as input data, in which h_c is the beam height between fasteners [mm] (see Figure 3.8).

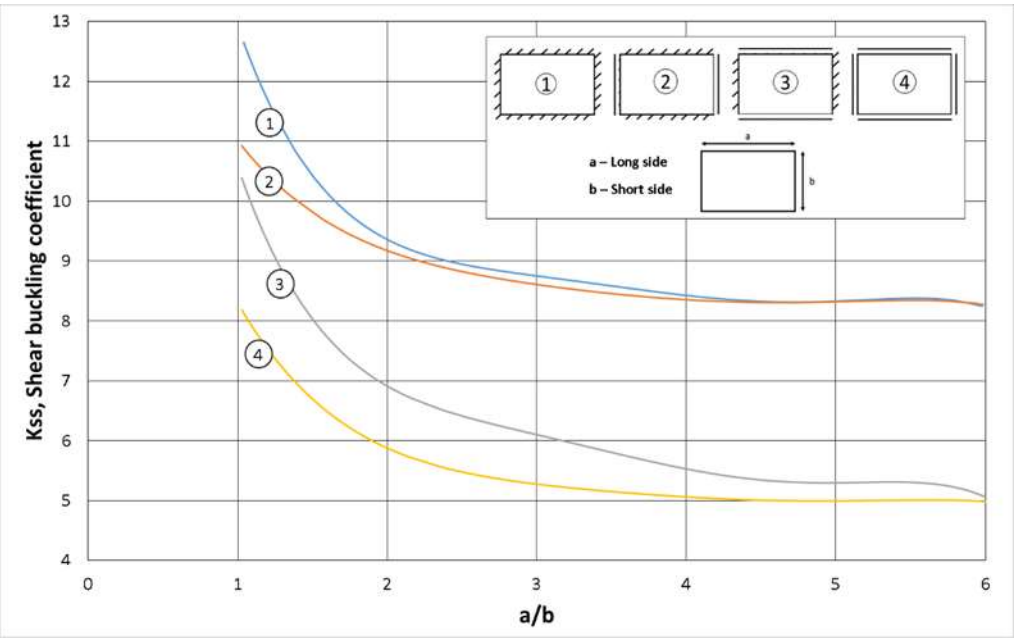

Figure 3.11 - Theoretical buckling coefficient for plates with simple supported edges (K_{ss}). Adapted from Niu, 2005, p. 460.

The value of C_1 is obtained with the graph presented in Figure 3.12, in which the input data is tan α (α is the angle between the neutral axes of panel's web and the direction of diagonal tension [degrees]).

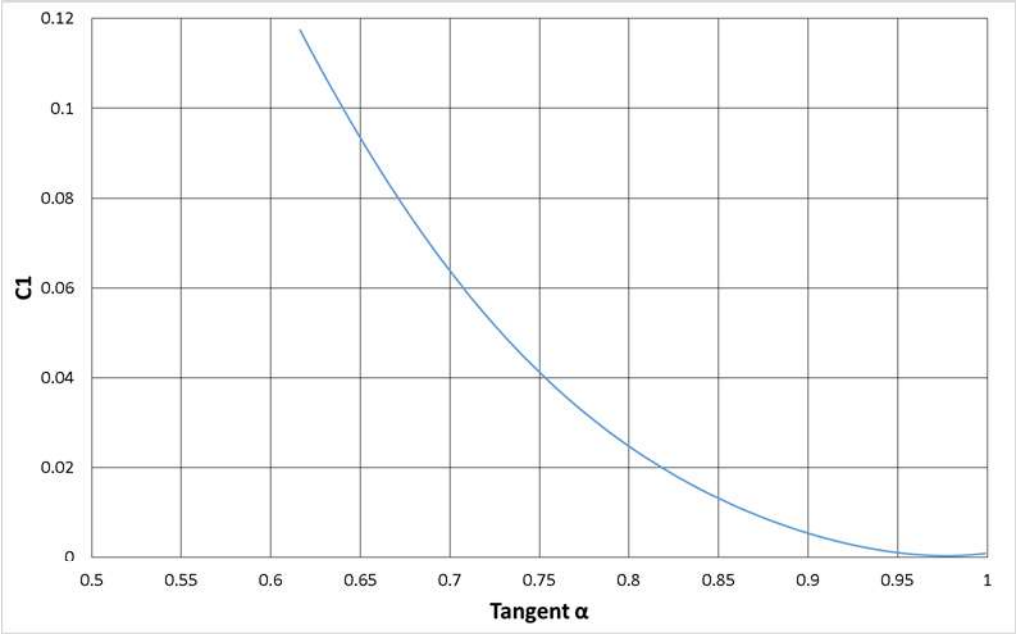

Figure 3.12 - Angle factor (C_1).
Adapted from Niu, 2005, p. 495

The value of $\tan\alpha$ can be found with the graph shown in Figure 3.13, in which the ration $\frac{fu}{f_s}$ is the input data, and f_u is the average stress in vertical stiffener [MPa].

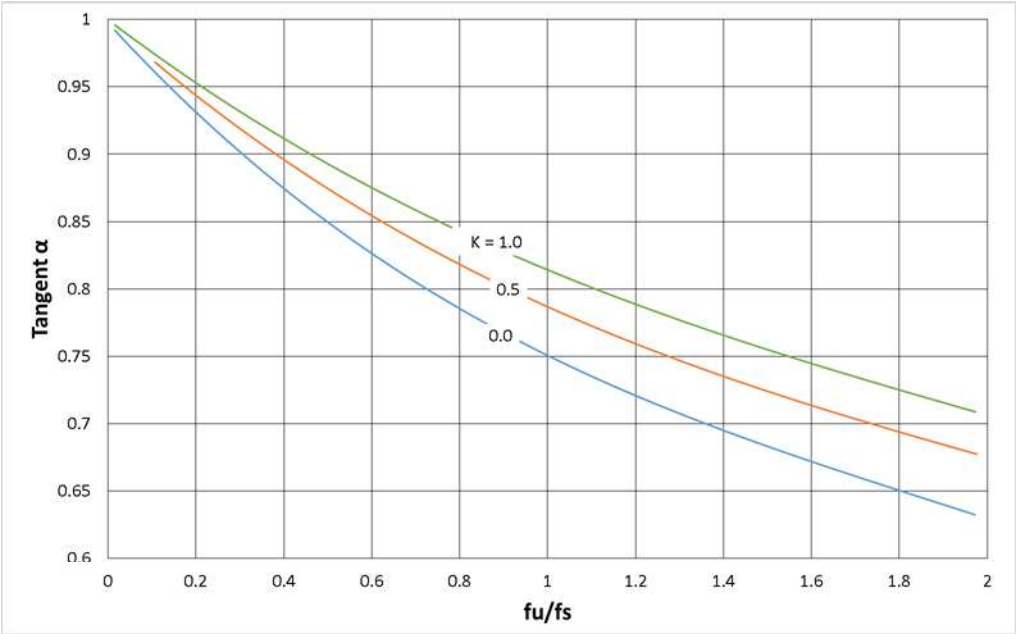

Figure 3.13 – Tangent of diagonal tension angle ($\tan\alpha$).
Adapted from Niu, 2005, p. 495.

The value of the ratio $\frac{fu}{f_s}$ can be reached using the graph given in Figure 3.14, using the ratio $\frac{A_{ue}}{d_c\, t}$, and the diagonal tension factor (k) as the input data. In which A_{ue} is the horizontal and vertical stiffeners effective area [mm^2] (Eq.(3.7)).

$$A_{ue} = \frac{A_u}{1 + (e/\rho)^2} \tag{3.7}$$

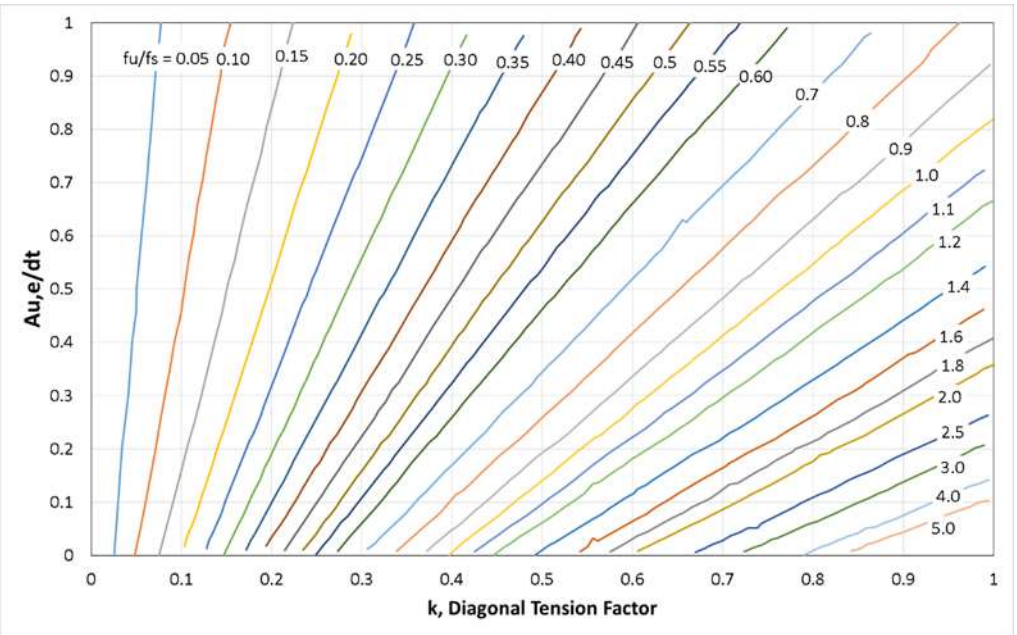

Figure 3.14 – Ratio of Stiffener Compression Stress to Web Stress.
Adapted from Niu, 2005, p. 491.

C_2 can be found using the graph from Figure 3.15, using the flange flexibility factor (wd) as the input data.

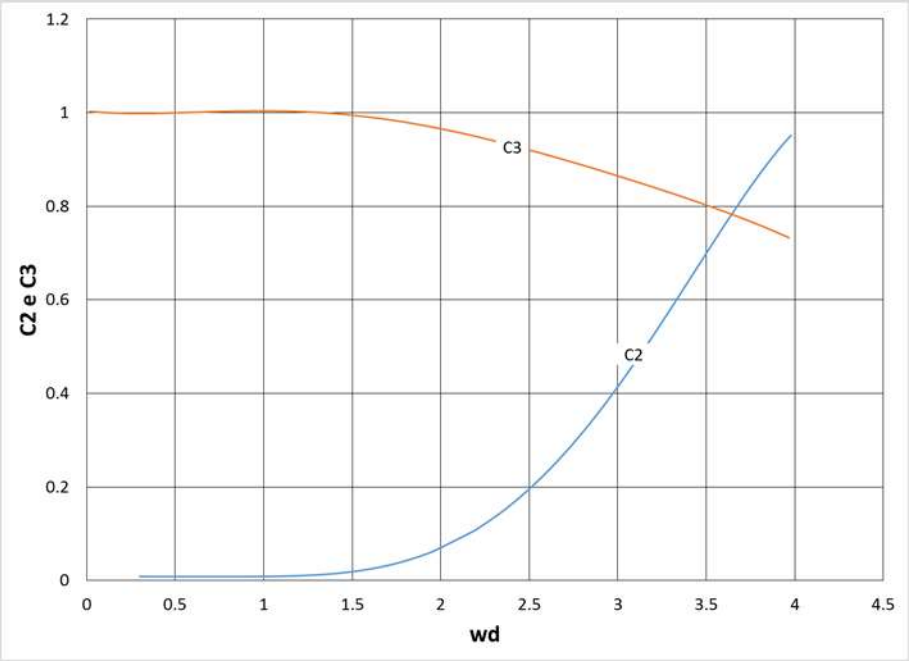

Figure 3.15 – Stress concentration factor (C_2).
Adapted from Niu, 2005, p. 495

The value of flange flexibility factor (wd) is calculated using Eq.(3.8).

$$wd = 0.7\, d \sqrt[4]{\frac{t}{(I_C + I_T)h_e}} \tag{3.8}$$

3.2 Composite Materials

Three different scales are used to evaluate the composite material depending on the characteristic or behavior under consideration. The first one is the micromechanics, which studies the interaction between the constituents in a microscopic level. In this study it is evaluated the constituent's stresses and strains, and local failures, as matrix failure (tension, compression and shear), fiber failure (tension, buckling and splitting), and the interface failure (debonding).

The second scale is the macromechanics, which consists in the analysis of the laminate as a homogenous material and the use of average properties in the analysis. The failure criterion is based on average stresses, and overall lamina strength, without referring to local failures. This study is applied in the form of lamination theory, which takes into account the laminate behavior based in the ply's properties and stacking sequence.

The third scale is on the structure or component level, which involves finite element analysis combined with the lamination theory and in the overall behavior of the structure (Daniel e Ishai, 1994).

3.2.1 Lamination Theory

The lamination theory is based on the macromechanics level, which considers the unidirectional lamina as a building block of the laminate. The principal coordinate system is shown in Figure 3.16 and the reference coordinate system is shown in Figure 3.17.

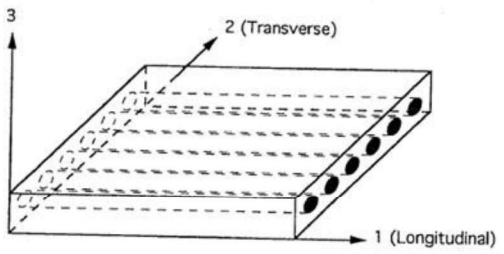

Figure 3.16 – Unidirectional lamina and principal coordinate system.
Daniel and Ishai, 1994, p. 21.

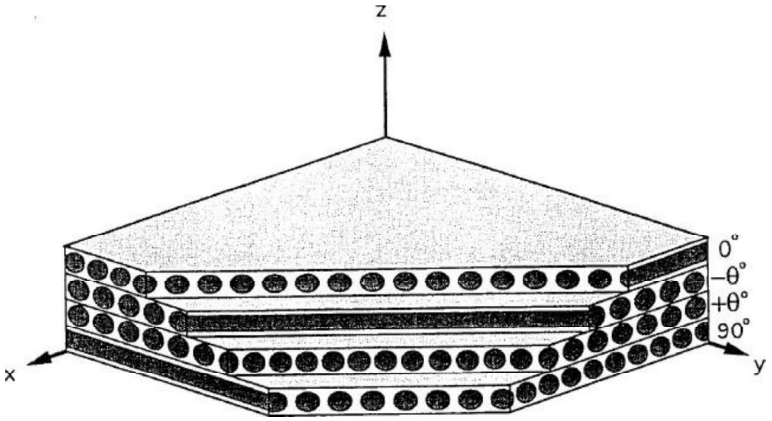

Figure 3.17 – Multidirectional lamina and reference coordinate system.
Daniel and Ishai, 1994, p. 22.

The ply is characterized by the properties presented in Eqs. from (3.9) to (3.18).

$$E_1 = V_f E_{1f} + V_m E_m \tag{3.9}$$

$$\nu_{12} = V_f \nu_{12f} + V_m \nu_m \tag{3.10}$$

$$E_2 = \frac{E_{2f} E'_m}{V_f E'_m + V_m E_{2f}} \tag{3.11}$$

$$E'_m = \frac{E_m}{1 - \nu_m^2} \tag{3.12}$$

$$G_{12} = \frac{G_{12f} G_m}{V_f G_m + V_m G_{12f}} \tag{3.13}$$

$$V_f = \frac{Volume\ of\ fibers}{Volume\ of\ composite} \tag{3.14}$$

$$V_m = \frac{Volume\ of\ matrix}{Volume\ of\ composite} \tag{3.15}$$

$$W_f = \frac{Weight\ of\ fibers}{Weight\ of\ composite} \tag{3.16}$$

$$W_m = 1 - W_f = \frac{Weight\ of\ matrix}{Weight\ of\ composite} \tag{3.17}$$

$$V_v = 1 - V_f - V_m = \frac{Volume\ of\ voids}{Volume\ of\ composite} \tag{3.18}$$

In which,

E_1, E_2, E_3 are the Young's modulus along the principal ply directions (see Figure 3.16) [MPa];

G_{12}, G_{23}, G_{13} are the shear modulus in 1-2, 2-3 e 1-3 planes (these are equals G_{21}, G_{32}, G_{31} respectively) [MPa];

$\nu_{12}, \nu_{23}, \nu_{13}$ are the Poisson's ratio (the first subscript denotes the loading direction, and the second one the strain direction; and these values are different $\nu_{21}, \nu_{32}, \nu_{31}$);

E_m, E_{1f} e E_{2f} are the Young's modulus of matrix and fiber in longitudinal and transversal direction, respectively [MPa];

V_f, V_m e V_v are the volume ratio for fiber, matrix and void;

W_f e W_m sare the weight ratio for fiber and matrix;

ν_m e ν_{12f} are the Poisson's ratio for matrix and fiber in longitudinal direction;

G_{12f} e G_m are the shear modulus for fiber and matrix [MPa].

The laminate is made up by unidirectional laminae stacked together in different orientations. The stacking sequence and fiber orientations will depend on the use of the component and the loads that it will carry. As mentioned before, for the macromechanics scale, the laminate is analyzed using the average properties (Nettles, 1994). In order to calculate these properties, first it is necessary to obtain the ABD matrix (see Eqs. (3.19) to (3.22)).

$$ABD = \begin{bmatrix} A & B \\ B & D \end{bmatrix} \tag{3.19}$$

$$A = \begin{bmatrix} A_{xx} & A_{xy} & A_{xs} \\ A_{yx} & A_{yy} & A_{ys} \\ A_{sx} & A_{sy} & A_{ss} \end{bmatrix} \tag{3.20}$$

$$B = \begin{bmatrix} B_{xx} & B_{xy} & B_{xs} \\ B_{yx} & B_{yy} & B_{ys} \\ B_{sx} & B_{sy} & B_{ss} \end{bmatrix} \tag{3.21}$$

$$D = \begin{bmatrix} D_{xx} & D_{xy} & D_{xs} \\ D_{yx} & D_{yy} & D_{ys} \\ D_{sx} & D_{sy} & D_{ss} \end{bmatrix} \tag{3.22}$$

The matrix A describes the membrane deformations of a laminate under in-plane loads, matrix D describes the membrane deformations of a laminate under pure bending loads, and matrix B describes the membrane-bending coupling (Kassapoglou, 2013). Usually the laminates are designed to be symmetric (matrix B is zero), balanced (Axs = Ays = 0), and with no coupling between bending and torsion (Dxs = Dys = 0). The balanced layups remove the membrane coupling between in-plane normal and shear behavior, and the symmetric laminates uncouple bending and membrane response, and prevent warping under thermal loading (Bailie, Ley and Pasricha, 1997).

In order to obtain the coefficients to build the ABD matrix, first it is necessary to calculate the reduced stiffnesses in the lamina principal axis, shown in Eq. from (3.23) to (3.26).

$$Q_{11} = \frac{E_1}{1 - \nu_{12}\nu_{21}} \tag{3.23}$$

$$Q_{22} = \frac{E_2}{1 - \nu_{12}\nu_{21}} \tag{3.24}$$

$$Q_{12} = \frac{\nu_{21}E_1}{1 - \nu_{12}\nu_{21}} = \frac{\nu_{12}E_2}{1 - \nu_{12}\nu_{21}} \tag{3.25}$$

$$Q_{66} = G_{12} \tag{3.26}$$

Then it is necessary to transform the reduced stiffnesses to the loading or reference stress coordinate system (x, y, z). This transformation can be performed using Eqs. (3.27) to (3.32).

$$Q_{xx} = m^4Q_{11} + n^4Q_{22} + 2m^2n^2Q_{12} + 4m^2n^2Q_{66} \tag{3.27}$$

$$Q_{yy} = n^4Q_{11} + m^4Q_{22} + 2m^2n^2Q_{12} + 4m^2n^2Q_{66} \tag{3.28}$$

$$Q_{xy} = m^2n^2Q_{11} + m^2n^2Q_{22} + (m^4 + n^4)Q_{12} - 4m^2n^2Q_{66} \tag{3.29}$$

$$Q_{xs} = m^3nQ_{11} - mn^3Q_{22} + (mn^3 - m^3n)Q_{12} + 2(mn^3 - m^3n)Q_{66} \tag{3.30}$$

$$Q_{ys} = mn^3Q_{11} - m^3nQ_{22} + (m^3n - mn^3)Q_{12} + 2(m^3n - mn^3)Q_{66} \tag{3.31}$$

$$Q_{ss} = m^2n^2Q_{11} + m^2n^2Q_{22} - 2m^2n^2Q_{12} + (m^2 - n^2)^2Q_{66} \tag{3.32}$$

$m = \cos(\theta)$ and $n = sen(\theta)$.

The coefficient from ABD matrix are calculated using the values mention before with Eqs. from (3.33) to (3.35).

$$A_{ij} = \sum_{k=1}^{n} Q_{ij}{}^{k} \, (h_k - h_{k-1}) \tag{3.33}$$

$$B_{ij} = \sum_{k=1}^{n} \frac{1}{2} Q_{ij}{}^{k} \, (h^2{}_k - h^2{}_{k-1}) \tag{3.34}$$

$$C_{ij} = \sum_{k=1}^{n} \frac{1}{3} Q_{ij}{}^{k} \, (h^3{}_k - h^3{}_{k-1}) \tag{3.35}$$

With i,j = x,y,s.

After the calculation of the coefficients from ABD matrix it is necessary to calculate matrix abd, the ABD inverse matrix (Eq.(3.36)).

$$abd = ABD^{-1} = \begin{bmatrix} a & b \\ b & d \end{bmatrix} \tag{3.36}$$

From the coefficients of abd matrix it is possible to calculate the equivalent properties from laminate in the reference coordinate system. The calculations are shown in Eqs. (3.37) to (3.46).

$$E_x = \frac{1}{h a_{xx}} \tag{3.37}$$

$$E_y = \frac{1}{h a_{yy}} \tag{3.38}$$

$$G_{xy} = \frac{1}{h a_{ss}} \tag{3.39}$$

$$\nu_{xy} = -\frac{a_{yx}}{a_{xx}} \tag{3.40}$$

$$\nu_{yx} = -\frac{a_{xy}}{a_{yy}} \tag{3.41}$$

$$\nu_{xy} = -\frac{a_{yx}}{a_{xx}} \tag{3.42}$$

$$\eta_{sx} = \frac{a_{xs}}{a_{ss}} \tag{3.43}$$

$$\eta_{xs} = \frac{a_{sx}}{a_{xx}} \tag{3.44}$$

$$\eta_{ys} = \frac{a_{sy}}{a_{yy}} \tag{3.45}$$

$$\eta_{sy} = \frac{a_{ys}}{a_{ss}} \tag{3.46}$$

3.2.2 Failure Theories

The failure theories for composite materials have been proposed to adapt and extend the isotropic failures theories to account for the anisotropy in stiffness and strength of the composite. All theories can be expressed in terms of the basic strength parameters in the principal material axis, and some theories do not account for interaction of stress components

while others do so to varying degrees. The following two failure theories are considered representative and most widely used (Daniel and Ishai, 1994)).

3.2.2.1 Maximum Strain Failure Theory

Equation (3.47) to (3.49) show the failure criteria.

$$\varepsilon_x < {\varepsilon_{xu}}^T \text{or } \varepsilon_x < {\varepsilon_{xu}}^C \tag{3.47}$$

$$\varepsilon_y < {\varepsilon_{yu}}^T \text{or} \varepsilon_y < {\varepsilon_{yu}}^C \tag{3.48}$$

$$|\gamma_{xy}| < \gamma_{xyu} \tag{3.49}$$

Where, $\varepsilon_{xu}{}^T$and $\varepsilon_{yu}{}^T$ are the ultimate longitudinal tensile and compressive strain, respectively; $\varepsilon_{xu}{}^C$ and $\varepsilon_{yu}{}^C$ are the ultimate transverse tensile and compressive strain, respectively; and γ_{xyu} is the ultimate in-plane shear strain.

3.2.2.2 Tsai-Wu Failure Theory

Equation (3.50) shows the failure criteria.

$$\frac{{\sigma_x}^2}{X^T X^C} + \frac{{\sigma_y}^2}{Y^T Y^C} - \sqrt{\frac{1}{X^T X^C}\frac{1}{Y^T Y^C}}\sigma_x\sigma_y + \left(\frac{1}{X^T} - \frac{1}{X^C}\right)\sigma_x + \left(\frac{1}{Y^T} - \frac{1}{Y^C}\right)\sigma_y + \frac{{r_{xy}}^2}{S^2} = 1 \tag{3.50}$$

Where, $X^T$and Y^T are the ultimate longitudinal tensile and compressive stress, respectively; X^C and Y^C are the ultimate transverse tensile and compressive stress, respectively; and S is the ultimate in-plane shear stress.

3.3 Post-buckling analysis in composite materials panels

The behavior of metallic reinforced panels in post-buckling regime is well known and has an established calculation methodology, NACA TN2661 (Kuhn, Peterson and Levin, 1952b). But the composite material reinforced panels have a different behavior after buckling, therefore several studies were performed in order to describe this behavior and propose a calculation method.

Agarwal, 1981 evaluated the post-buckling behavior of composite (graphite-epoxy) multibay shear webs. He designed several test specimens and tested them using static and fatigue loads. The results were compared with numerical simulation, using large deflection analysis to predict the post-buckling behavior. His conclusion was that the composite material shear webs have significant post-buckling strength and different failure modes when compare to metal shear webs. Therefore, the calculation method used to design metallic reinforced panel, even when they have modification to account for the anisotropy of the material, are not good for predicting post-buckling behavior for composite material reinforced panels.

Wittenberg, et al., 2001 adapted Kunh's method for calculating metallic shear panels during the post-buckling, making it consider the anisotropy of the material. The adapted method would be used in the design of stiffened Glare (GLAss REinforced aluminum) shear panels. The new methodology was verified comparing its results to experimental data (two panels were built and tested until failure). Afterwards a finite element model was developed, to predict panel's responses during the tests. The FEM results showed very good agreement with experimental data, giving confidence in replacing very costly actual panel tests with computer simulations.

As the work previous described, Jodoin et al., 2002 also adapted the metallic reinforce panel method for diagonal tension in order to be used for Glare shear panels. He tested several panels using GLARE 3, GLARE 4, and 2024-T3 aluminum with different thickness. The comparison of the results from the tests and the adapted methodology have shown that the NACA-based methodology can be used to predict GLARE web stress/strain reactions up to its yield point.

In order to reduce weight in commercial aircrafts, the European Commission supported the program COCOMAT (Improved MATerial Exploitation at Safe Design of COmposite Airframe Structures by Accurate Simulation). The team aimed to achieve their goal by exploiting considerable reserves in primary fiber composite fuselage structures through an accurate and reliable simulation of post-buckling up to collapse. Therefore, two analysis tools

were developed, one focusing in accuracy but requiring more time to run, and the other presenting approximate results but with faster calculations. They were calibrated comparing their results to tests results. The specimens tested were designed under different objectives. The numerical calculations have been successfully validated with experimental data up to the first global buckling. For the simulation of the deep post-buckling region, degradation must be considered (Degenhardt et al., 2008).

Herrero, 2007 developed a non-linear finite element models in order to enhance composite structures design. He exploited the post-buckling capacity of these structures combining the finite element models with continuum damage mechanism models, to simulate the failure and subsequent material property degradation. The results from finite element models were compared with experimental data. Deformation results were taken from rosetts strain gages installed at the center of panels, and the out of plane deformation were recorded with photo-sensitive digital image system (ARAMIS). The conclusion was the finite element model presented good correlation with test data, but in order to improve finite element model accuracy, initial imperfections and material degradation were introduced in the model. The results showed an improvement in finite element model and in the test results correlation.

The work developed by Melo, 1993 was an experimental study about the influence of fiber orientation in shear post-buckling behavior. Three specimens were built using two different material and the following angles between the fiber and the applied load: 0º, 45º and 90º. The conclusion was that the laminate with plies oriented in 0º show more strength and stiffness than the one in 45º and in 90º. The 45º laminate presents large deformation before failure and is stiffer than the 90º laminate. And the 90º laminate presents more strength than the 45º laminate but is the first to fail.

3.4 Finite Element Model using NASTRAN®

3.4.1 Linear Buckling

According to NASTRAN, 2012b, the problem of linear buckling is defined by including the effect of the differential stiffness to the linear stiffness matrix. The differential stiffness results from including the higher-order terms of the strain-displacement relationships in the matrix. The differential stiffness matrix, or geometric stiffness matrix, is a function of the geometry, element type, and applied loads.

The overall stiffness matrix is represented in Eq. (3.51), the linear stiffness matrix in Eq. (3.52) and the differential stiffness matrix in Eq.(3.53).

$$[K] = [K_a] + [K_d] \tag{3.51}$$

$$[K_a] = \sum_{i}^{n} K_{a_i} \tag{3.52}$$

$$[K_d] = \sum_{i}^{n} K_{d_i} \tag{3.53}$$

The total potential energy is shown in Eq. (3.54).

$$[U] = 0.5\{u\}^T[K_a]\{u\} + 0.5\{u\}^T[K_d]\{u\} \tag{3.54}$$

For the equilibrium of the system, the total energy must have a stationary value, as presented in Eq. (3.55).

$$\frac{d[U]}{du_i} = [K_a]\{u\} + [K_d]\{u\} = [K_a]\{u\} + P_a[K_d]\{u\} = \{0\} \tag{3.55}$$

In which u_i is the displacement of i-th degree of freedom, P_a is the applied load.

In order to Eq. (3.54) to have a non-trivial solution, the following relationship (Eq.(3.56)) has to be true.

$$\det([K_a] + P_a[K_d]) = \{0\} \tag{3.56}$$

Eq. (3.55) is only satisfied for some values of P_a, and these are the critical buckling load. The number of buckling loads obtained from the finite element model is equal to model's degree of freedom. This is represented by Eq. (3.57).

$$P_{cr_i} = \lambda_i P_a \tag{3.57}$$

Therefore, Eq. (3.56) can be rewrite as Eq. (3.57) in the form of eigenvalue problem. Once the eigenvalues are obtained, the buckling loads can be reached by Eq. (3.58).

$$\det([K_a] + \lambda_i[K_d]) = \{0\} \tag{3.58}$$

3.4.2 FEM composites

According to NASTRAN, 2012b, a two-dimensional composite material is defined as a stacked group of laminae arranged to form a flat or curved plate or shell. A laminate is a stack of these individual lamina arranged with the principal directions of each lamina oriented in a particular direction as shown in Figure 3.18.

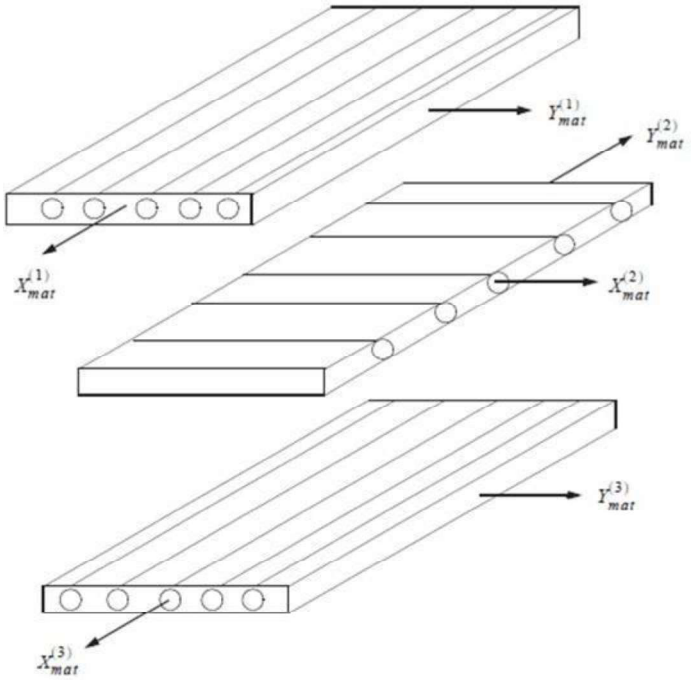

Figure 3.18 - Laminae arrangement for a laminate.
NATRAN 2012b, p. 223.

The laminae are bonded together with a thin layer of bonding material that is considered to be of zero thickness. Each lamina can be modeled as an isotropic material, two-dimensional anisotropic material, or orthotropic material. The assumptions inherent in the lamination theory are each lamina is in a state of plane stress, the bonding is perfect, two-dimensional plate theory can be used, and linear variation of strain through the laminate thickness is assumed (NASTRAN, 2012b).

It is possible to request as output: stresses and strains for the equivalent plate, force resultants, stresses and/or strains in the individual lamina, including approximate interlaminar shear stresses in the bonding material output, and a failure index table.

4

4 METHODOLOGY

This study methodology is divided in five steps presented hereafter, and a workflow is presented in Figure 4.1.

The first step is to build a Finite Element Model (FEM) for a metallic reinforced panel with horizontal and vertical stiffeners. One side of the panel is fixed, and a force is applied on the opposite side. A linear static analysis, a linear buckling analysis and a non-linear analysis are performed.

The second step is a comparison between results from the hand calculation for the diagonal tension using NACA TN2661 (Kuhn, Peterson and Levin, 1952a) method and FEM results, in order to guarantee that the model is calibrated. The values of maximum stress in the middle of panel (f_{smax} Eq. (3.4)), and shear nominal stress in the web (f_s Eq. (3.5)) from the hand-calculation are compared with the same results from FEM. Then a comparison between the buckling load obtained from the linear and non-linear analyzes is performed. The load from linear analysis is calculated by multiplying the first eigenvalue found in the linear buckling analysis by the load applied in the panel. For the non-linear analysis, the buckling load is reached using the load-displacement graph, constructing one line for the first slope and another one for the second slope. The place where the lines meet is the buckling load, as described in Arakaki and Faria, 2016. If the differences are smaller than the error previous defined, it is possible to continue to the next step. Otherwise, the FEM must be modified in order to achieve that error. It can be changed the boundary conditions, the region, or nodes of load application, or the stiffeners element (linear element or plate element). By the end of this step the model and mesh are considered calibrated.

Step three is a verification of the use of the calibrated mesh to build a FEM for the composite reinforced panel. In order to perform the verification, two models are built: one with the equivalent properties for the layup chosen, and the other one modeling each layer and using the material properties of the tape. The buckling load from linear buckling analysis, and the load step when the diagonal tension is complete, and the panel's web redistribute the compressive load to the stiffeners from the non-linear analysis, were compared. If the differences are smaller than the error previous defined, it is possible to continue to the next step. Otherwise, the FEM must be modified in order to achieve that error. It can be changed the laminate or the tape material, or it is possible to return to step two and recalibrate the model.

Step four consists in select the stacking sequence and the angle of fiber orientations for the layups, which have to be symmetric and balanced. For each layup, a FEM is created modeling each layer and using the material properties of the tape. Also, for each layup it will be applied several different loads values at the panel, in order to evaluate the reinforced panel behavior for different loads magnitude. A non-linear analysis for each model is performed, and the failure index of the step when the diagonal tension is complete, and the panel's web redistribute the compressive load to the stiffeners for all of them is compared. The layup that presents the lowest values for the failure index for all the loads is chosen to be the laminate having the best post-buckling behavior.

In step five a metallic reinforced panel FEM with the same weight that the composite reinforced panel layup chosen in step four is built. Then compare the buckling load from linear buckling analysis, and the load step when the diagonal tension is complete, and the panel's web redistribute the compressive load to the stiffeners from the non-linear analysis, in order to determine which one has the best behavior for post-buckling analysis.

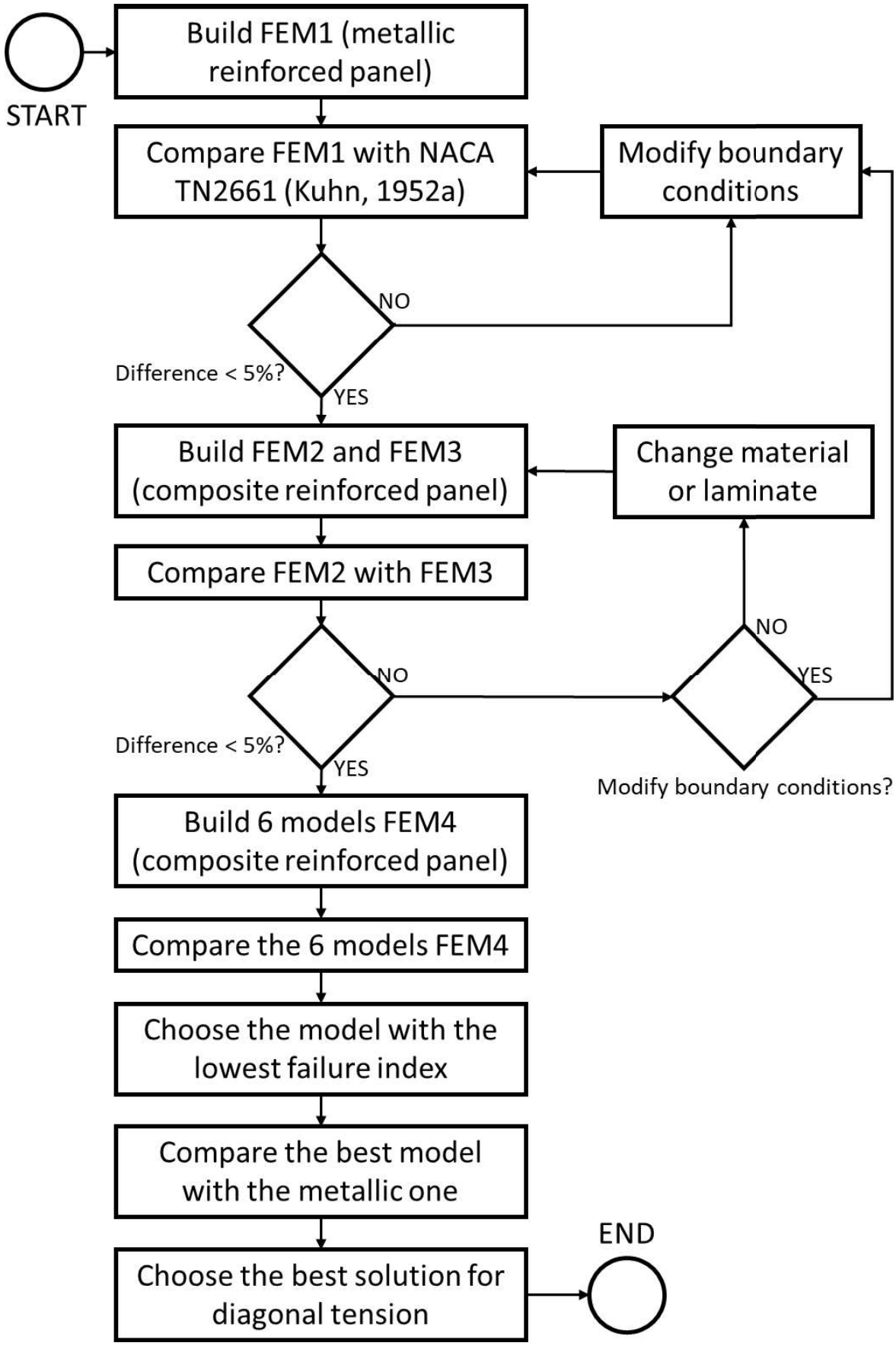

Figure 4.1 – Methodology workflow.

5

5 DISCUSSION

5.1 Metallic reinforced panel FEM

The first step of this study was to build a FEM for the metallic reinforced panel with horizontal and vertical stiffeners. The materials and dimensions for the panel and stiffeners, and the load applied in the structure, were taken from an example of diagonal tension calculation presented in Bruhn, 1973. The materials are shown in Table 5.1.

Table 5.1 - Metallic reinforced panel materials.

Material	
Web	Aluminum 2024 T3
Horizontal Upper Stiffener	Aluminum 7075-T3 Extruded
Horizontal Lower Stiffener	Aluminum 7075-T3 Extruded
Vertical Stiffener	Aluminum 7075-T3 Extruded

A schematic 3D model of the reinforced panel components and dimensions is presented in Figure 5.1. The panel's web thickness is shown in Table 5.2. The geometries of the horizontal and vertical stiffeners are presented in Figure 5.2 and Tables 5.3, 5.4 and 5.5.

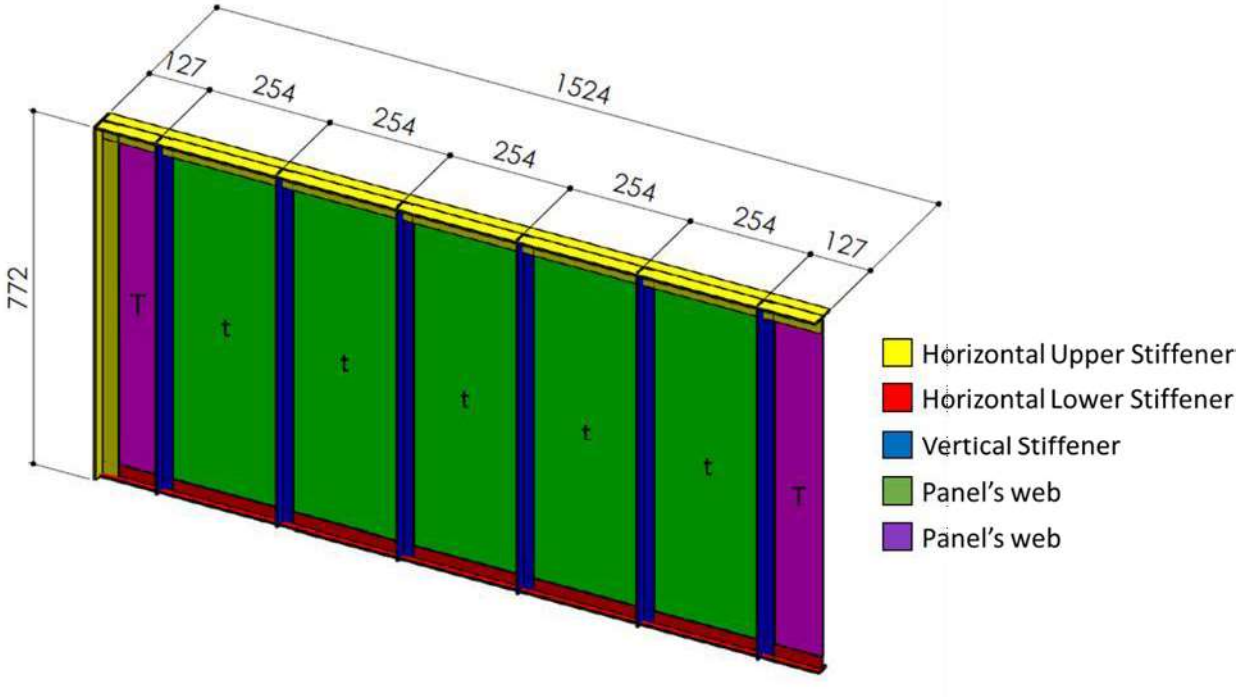

Figure 5.1 - Metallic reinforced panel 3D model – geometry (all dimensions are in mm).

Table 5.2 - Metallic reinforced panel dimensions.

Panel's web thickness	
t	0.635 mm
T = 2*t	1.270 mm

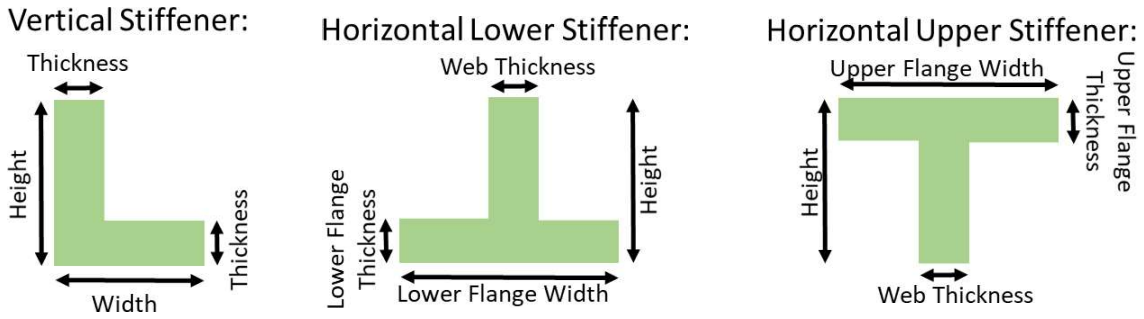

Figure 5.2 – Stiffeners geometry.

Table 5.3 - Metallic reinforced panel dimensions – Vertical Stiffeners.

Dimensions – Vertical Stiffeners	
Thickness	3.175 mm
Height	25.400 mm
Width	25.400 mm

Table 5.4 - Metallic reinforced panel dimensions – Upper Horizontal Stiffeners.

Dimensions – Upper Horizontal Stiffeners	
Web Thickness	3.97 mm
Height	38.10 mm
Upper Flange Width	58.74 mm
Upper Flange Thickness	3.97 mm

Table 5.5 - Metallic reinforced panel dimensions – Lower Horizontal Stiffeners.

Dimensions – Lower Horizontal Stiffeners	
Web Thickness	2.38 mm
Height	29.37 mm
Lower Flange Width	29.37 mm
Lower Flange Thickness	2.38 mm

The FEM was built using the software FEMAP 11.2® as pre- and post-processor and NASTRAN® as the solver. The panel's web was modeled using two-dimensions, four-nodes plate elements CQUAD4, which uses plane stress theory, capable of carrying in-plane forces, bending forces, and transverse shear forces (NASTRAN, 2012a). The vertical and horizontal stiffeners were modeled using one-dimension elements that connects two grid points CBAR, which is a straight prismatic element with axial, bending, and torsional stiffness (NASTRAN, 2012a). The CBAR element was chosen because the change in stiffener geometry using CBAR is easier to perform than it would be if it was modeled as plate elements. Consequently, the model is more versatile. Following the boundary conditions applied by Braz, 2018, on the left-hand side of the panel, fixed boundary conditions were applied in the last column of nodes.

Based on an example presented in Bruhn, 1973, a force of 60075 N was applied in the –Y direction on the right-hand side of the panel. The FEM is shown in Figure 5.3.

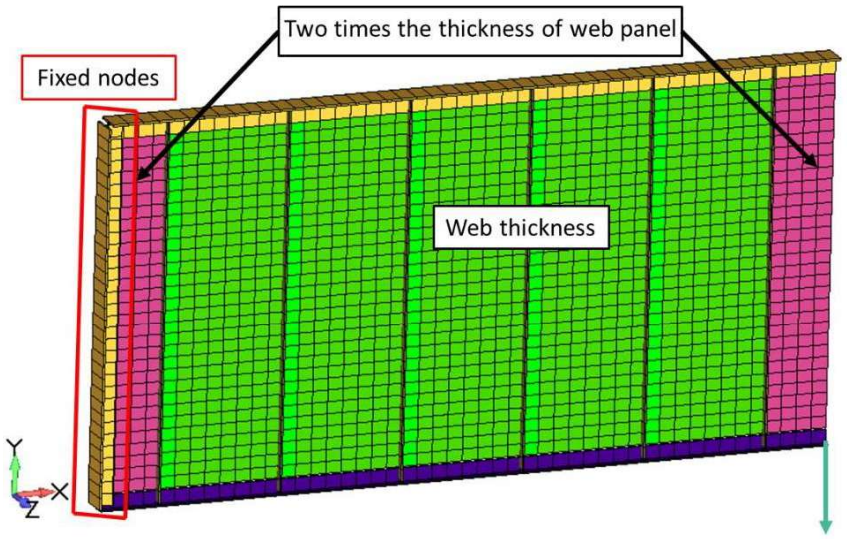

Figure 5.3 - Metallic reinforced panel FEM preliminary model.

It was performed a static analysis (SOL101) to evaluate the stress in the panel's web, a linear buckling analysis (SOL105) to calculate the buckling load, and a non-linear analysis including large displacements (SOL106) to evaluate the post-buckling behavior of the structure. The results obtained from the model and the hand calculation for diagonal tension using NACA TN2661 method (Kuhn, Peterson and Levin, 1952a) were compared, as described in Section 4, Methodology. Some modifications had to be performed in the model in order to better represent the problem and, therefore, reduce the differences found. On the right-hand side of the panel, a condition of displacement only in Y direction was applied in the first column of nodes. Also, the adjacent elements of the CBAR elements, representing the horizontal stiffeners, had their thickness increased. Therefore, these elements represent the web thickness and the stiffener thickness together. Figure 5.4 illustrates the modifications performed in the model.

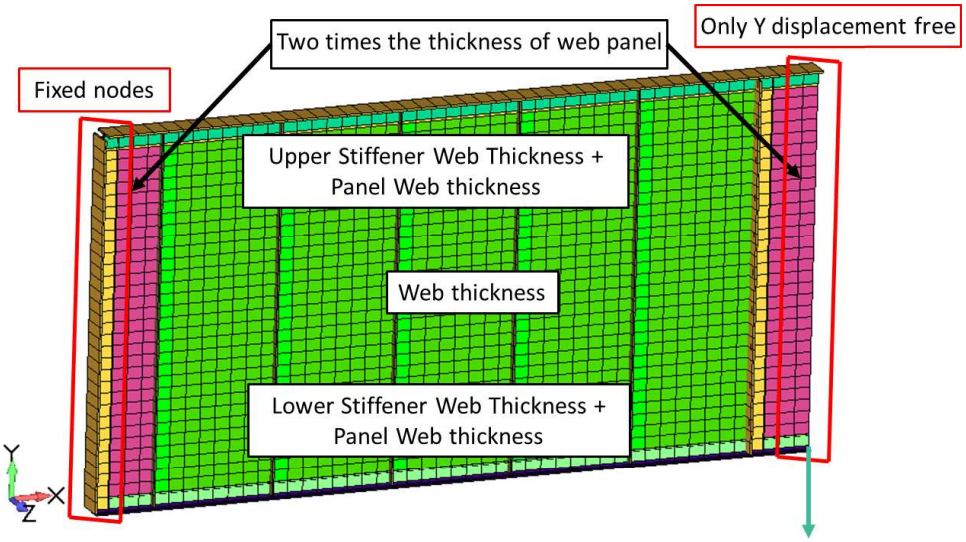

Figure 5.4 - Metallic reinforced panel FEM final model.

The same three analyses (SOL101, SOL105 and SOL106) were performed for the final model. Comparisons between the simulation results and hand calculation are presented hereafter.

The value of the average shear stress from FEM was compared with the maximum stress in the middle of panel (f_{smax}), calculated using Eq. (3.4) from the section 3 Bibliography Review. The comparison is shown in Figure 5.5 and Table 5.6.

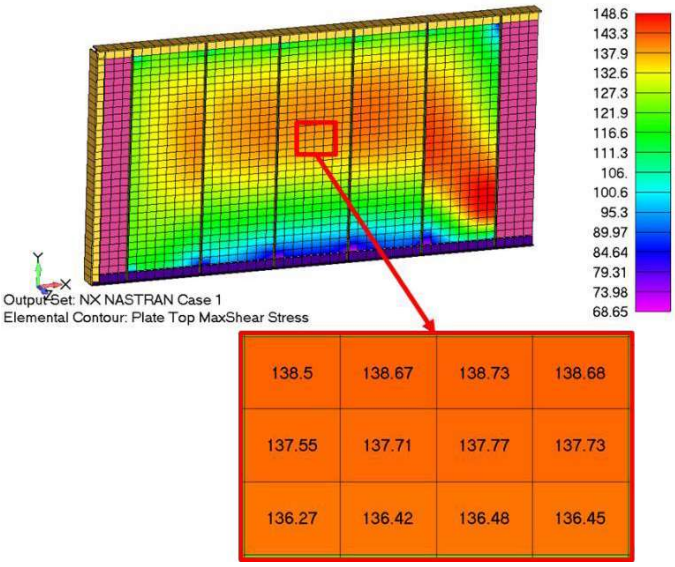

Figure 5.5: FEM maximum stress in the middle of panel (units in MPa).

Table 5.6 - Comparison between shear stress from FEM and from NACA TN2661 (Kuhn, Peterson and Levin, 1952a) method in the middle of the web.

FEM shear stress	**NACA TN2661 (Kuhn, Peterson and Levin, 1952a) shear stress (f_{smax})**	**Difference**
137.58 MPa	134.21 MPa	2.51%

The value of the shear nominal stress in the web (f_s) calculated using Eq. (3.5) from section 3 Bibliography Review, was compared with the FEM average shear stress in the region of the web where buckling occurs (for the first eigenvalue buckling mode). Figure 5.6 presents the FEM average shear stress in the web, and the comparison is shown in Table 5.7.

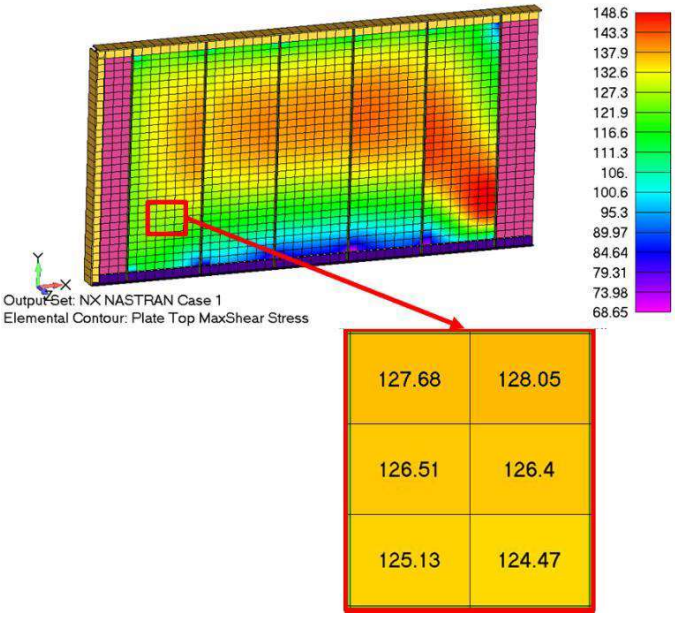

Figure 5.6: FEM average shear stress in the web, region of first eigenvalue buckling mode (units in MPa).

Table 5.7 - Comparison between shear stress from FEM and from NACA TN2661 (Kuhn, Peterson and Levin, 1952a) method.

FEM shear stress	NACA TN2661 (Kuhn, Peterson and Levin, 1952a) Shear nominal stress in the web (f_s)	Difference
126.37 MPa	126.42 MPa	0.04%

Using the results from the linear buckling analysis it is possible to determine the buckling load for the metallic reinforced panel. Figure 5.7 shows the first eigenvalue buckling mode.

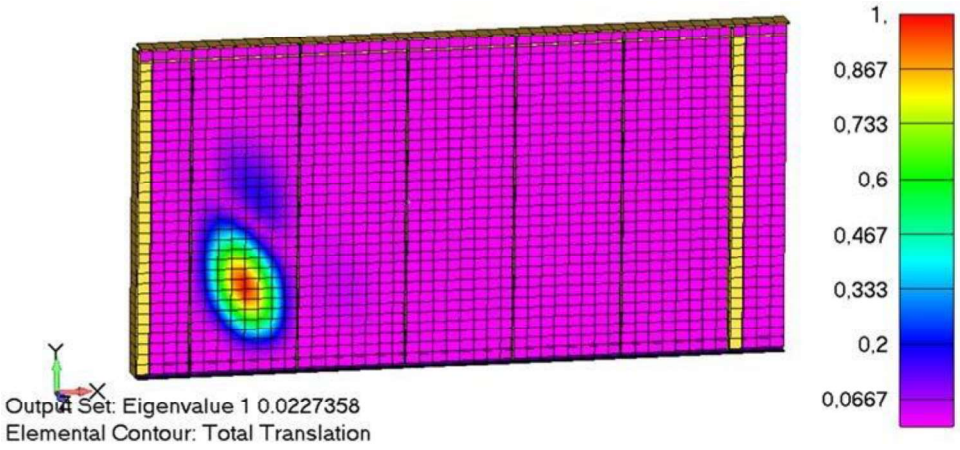

Figure 5.7: Metallic reinforced panel first eigenvalue buckling mode.

The buckling load is calculated using Eq. (3.57) presented in section 3 Bibliography Review:

$$P_{cr_i} = \lambda_i \, P_a = 60075N * 0.0227358 = 1365.85N$$

For the non-linear analysis (SOL106) the determination of the buckling load was performed plotting the non-linear load versus the total displacement of one node (it was chosen the one with greater displacement in the buckling region from the linear buckling analysis SOL105), as mentioned by Arakaki and Faria, 2016. On the plot load *vs*. displacement for the non-linear analysis (SOL106), a line A–A tangent to the first linear ramp was traced. Then a line B–B tangent to the second linear ramp, where there is a significant change in the rigidity, were also drawn (Figure 5.8). Zooming into the non-linear region of the same plot, the buckling load was obtained by the intersection of these two lines, as showed in Figure 5.9.

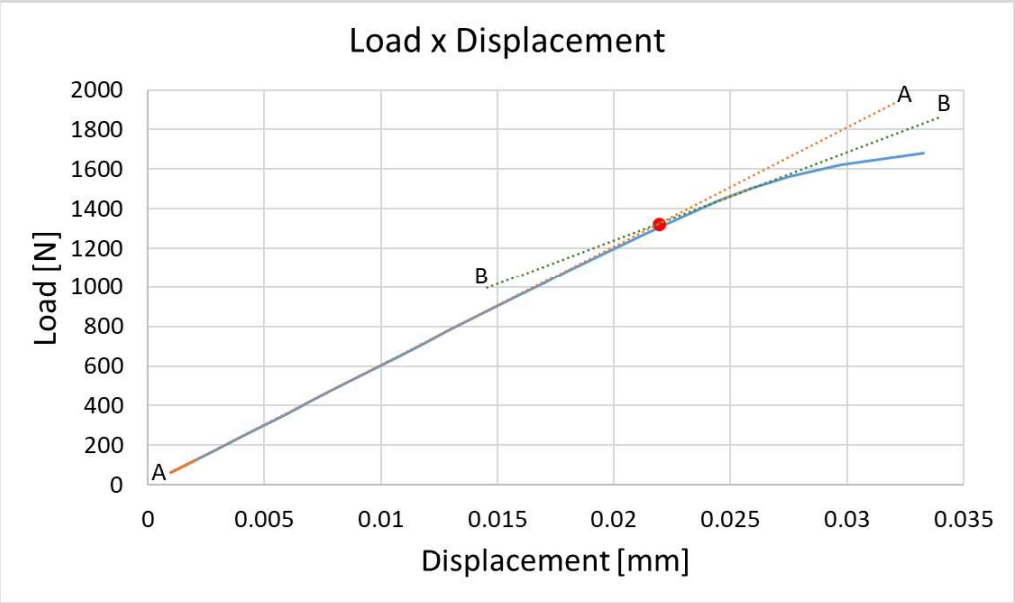

Figure 5.8 - Non-linear analysis load-displacement graph.

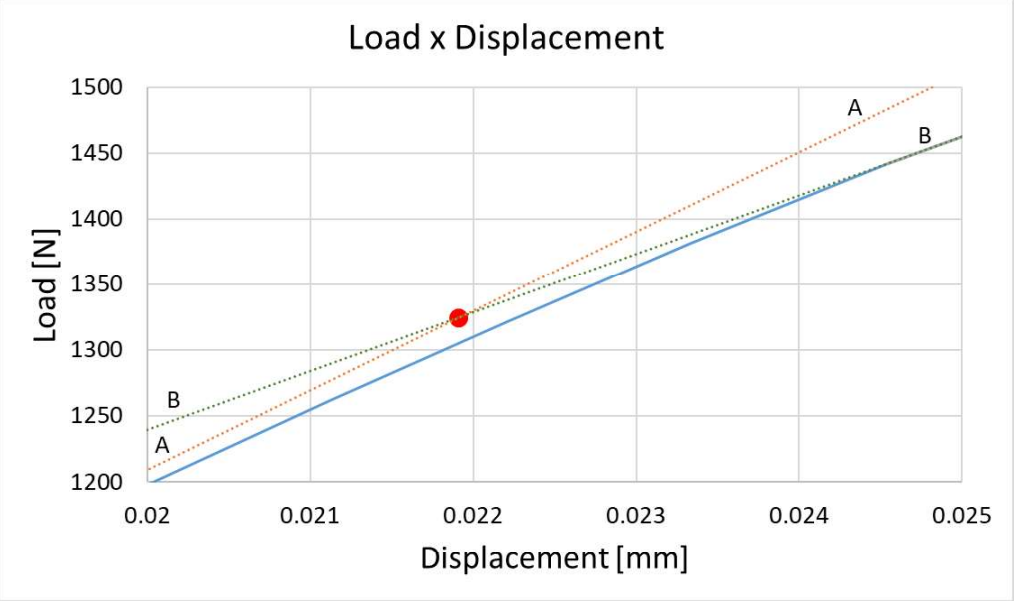

Figure 5.9 - Non-linear analysis load-displacement graph (zoom in the region where lines A-A and B-B cross).

The comparison between buckling loads obtained from the linear buckling (SOL105) and non-linear analysis (SOL106) is presented in Table 5.8.

Table 5.8 - Comparison between buckling loads from linear buckling analysis and non-linear analysis.

Linear buckling analysis	Non-linear analysis	Difference
1365.85 N	1324.36 N	3.13%

The results from comparison between FEM and hand calculation for diagonal tension using NACA TN2661 (Kuhn, Peterson and Levin, 1952a) method, (Tables 5.6 and 5.7), and the comparison between linear buckling and non-linear analysis, (Table 5.8), have shown that the greatest difference was 3.13%. These encouraging results create the necessary confidence to use the FEM model in the following analyses.

The reinforced panel post-buckling behavior was also analyzed from the non-linear simulation (SOL106). In this analysis, the panel total load (60075 N) was divided into 100 increments of 600.75 N, that were successively applied in the model. Therefore, at each 0.01 increment that occurs in the model, a load of 600.75 N is added to the reinforced panel (NASTRAN, 2012c).

The complete diagonal tension phenomenon was considered to occur when diagonal folders were visually formed in the panel's web. Figure 5.10 shows the load step where it occurred.

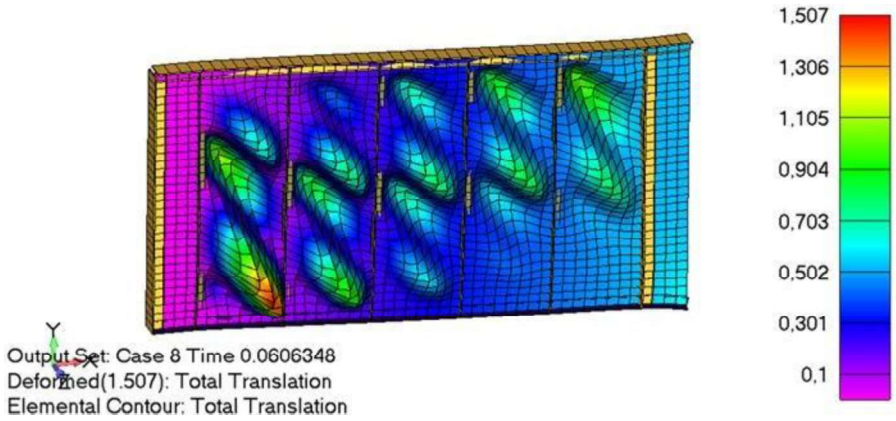

Figure 5.10 - Non-linear analysis – complete diagonal tension (deformations are plotted to scale at 150 times their actual value).

The complete diagonal tension load occurs when the panel's web redistributes the compressive load to the stiffeners. And it is obtained by multiplying the step where first occurs diagonal tension by the total load applied in the reinforced panel. Consequently, this load is calculated in Eq. (5.1):

$$0.0606348 * 60075N = 3642.64N \tag{5.1}$$

In order to check if this result was correct, two other verifications were performed. The first one was an analysis of the stress state of one element in the buckling region, using the non-linear solution (SOL106). Minimum Principal Stress (Min Prc), Maximum Principal Stress (Max Prc), and Maximum Shear Stress (Max Shear) were considered. Figure 5.11 shows these stresses plotted as functions of the applied load.

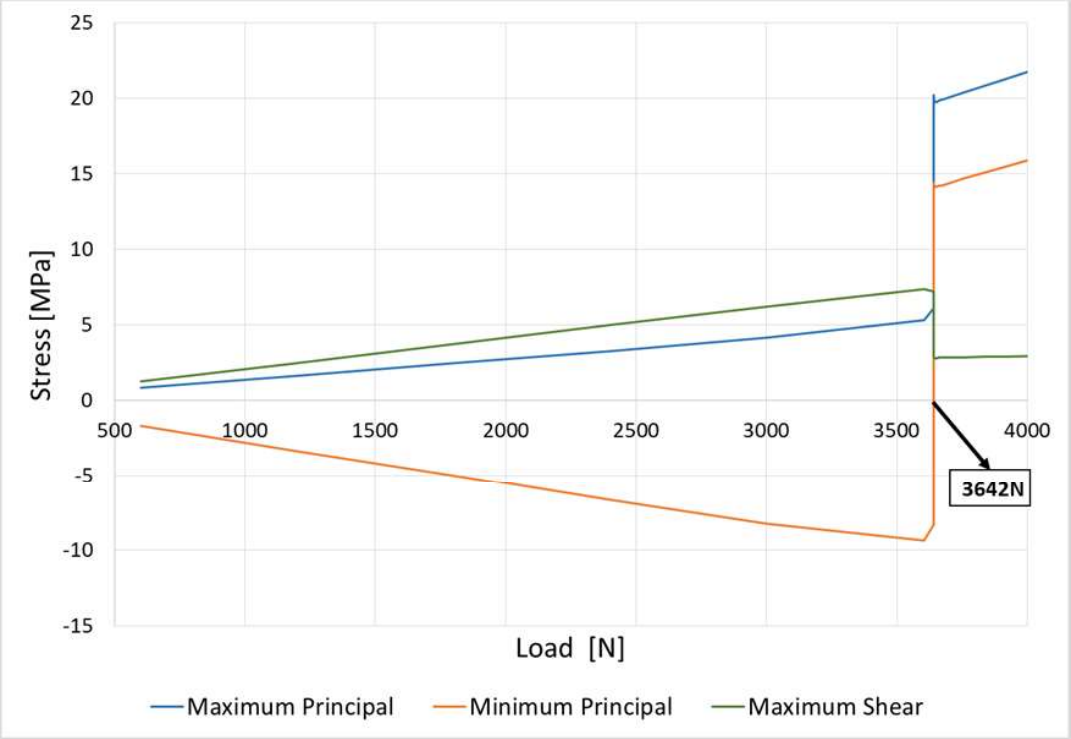

Figure 5.11 - Principal stresses during load increment.

In Figure 5.11, all these stresses (Max Prc, Min Prc and Max Shear) experience sharp variations on their values at the load 3642 N. The explanation for these changes is the diagonal tension field. When the panel's web buckles and it cannot hold compression stress anymore, diagonal

folds are formed in the web, which is further loaded only in tension. The shear stress is distributed for the stiffeners (Niu, 2005).

The second verification was an evaluation of the load that the horizontal stiffeners were carrying during load application. It was chosen four elements, two from the upper horizontal stiffener and the others from the lower horizontal stiffener, and the results were plotted in a graph. For the linear static analysis, the axial stresses in the linear element representing the stiffeners in the end of the analysis were taken. These values were plotted in the graph and a line was traced until the zero (at the load step zero the axial stress in the stiffener is also zero). For the non-linear analysis the axial stresses in the linear element representing the stiffeners were taken for each step of the analysis and these values were plotted against the load. The final result can be seen in Figure 5.12.

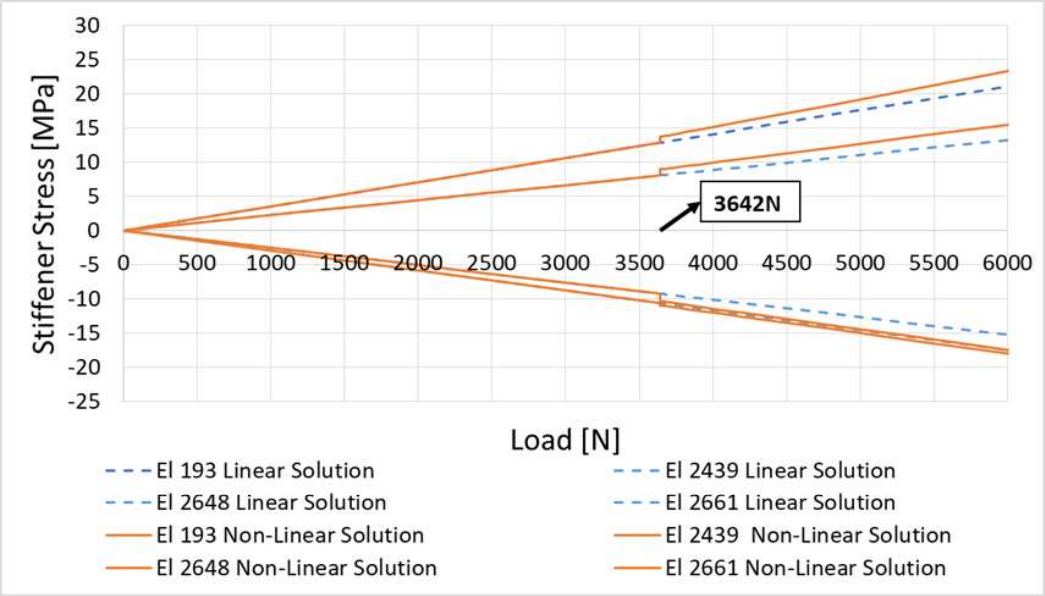

Figure 5.12 - Stress on the stiffener with the increase of the load.

The dashed line represents the axial stresses for the linear analysis, and the solid line represents the axial stresses for the non-linear analysis. It can be seen that for the load of 3642 N there is a discontinuity in the stress for the non-linear analysis, which means that at this load step the stiffeners start carrying more load than they would in the linear analysis. Therefore, this is the load step when the diagonal tension is complete, and the panel's web redistribute the compressive load to the stiffeners (Niu, 2005).

5.2 Composite Material Reinforced Panel versus Isotropic Reinforced Panel

The calibrated mesh aforementioned was used to build two FEM (with the same geometry) for the composite reinforced panel, model 1: modeling each layer and entering the material properties of the tape, and model 2: with the equivalent properties for the layup selected. It was chosen a carbon/epoxy tape, $[45/-45/0/90]_S$, balanced and symmetric. The choice of using 0º, +45º, -45º and 90º fiber orientation is due to the recommendation made by Bailie, Ley and Pasricha, 1997. They affirm that the laminate will be fiber dominant with the use of at least 10% of its plies in 0º, +45º, -45º and 90º. The balanced layups were chosen to remove the membrane coupling between in-plane normal and shear behavior, and the choice of use symmetric laminate is to uncouple bending and membrane response, and to prevent warping under thermal loading (Bailie, Ley and Pasricha, 1997). They also affirm that laminates should be symmetric and balanced to maximize buckling strengths.

Tables 5.9 and 5.10 present the properties and allowable for the carbon/epoxy tape chosen. The FEM material direction was aligned with the +X direction of global coordinate system, which means the tapes oriented in 0º were aligned with the +X direction.

Table 5.9 - Carbon/epoxy tape mechanical properties (Daniel and Ishai, 1994).

Material	**E1 [MPa]**	**E2 [MPa]**	**G12 [MPa]**	**ν12 [MPa]**	**t [mm]**	**Density [g/mm^2]**
Tape carbon/epoxy (AS4/APC2)	142000	10300	7100	0.27	0.19	0.00158

Table 5.10 - Carbon/epoxy tape allowable properties (Daniel and Ishai, 1994).

Material	**Xt [MPa]**	**Xc [MPa]**	**Yt [MPa]**	**Yc [MPa]**	**S12 [MPa]**	**S13 [MPa]**
Tape carbon/epoxy (AS4/APC2)	2280	1440	57	228	71	97

The equivalent properties for the stacking sequence and tape material above-mentioned, is shown in Table 5.11. Because the value of Ex is equal to Ey, an isotropic material was used n the FEM with the laminate equivalent properties.

Table 5.11 -Equivalent property - Tape carbon/epoxy $[45/-45/0/90]_S$

Equivalent Properties	
Ex	56675.5 [MPa]
Ey	56675.5 [MPa]
Gxy	22039.8 [MPa]
νxy	0.286
νyx	0.286

The materials and dimensions for the reinforced panels can be seen in Tables 5.12 to 5.16. The material for the stiffeners were changed from aluminum to steel, and their thickness (web and flange) were doubled, and the load applied in the reinforced panel was altered from 60075N to 143802N. These modifications were necessary to guarantee that a post-buckling behavior would occur in the reinforced panel even with the increase in web's thickness from 0.635mm to 1.52mm. All the other panel's dimension (height, width, etc) were kept the same.

Table 5.12 - Reinforced panels materials.

Material	
Web (model 1)	Tape carbon/epoxy $[45/-45/0/90]_S$
Web (model 2)	NA (it was used the Young's modulus equal to the composite model) E = 56675.5 MPa
Horizontal Upper Stiffener	Steel 4043
Horizontal Lower Stiffener	Steel 4043
Vertical Stiffener	Steel 4043

Table 5.13 - Reinforced panels dimensions.

Panel's web thickness	
t	1.52 mm
T = 2*t	3.04 mm

Table 5.14 - Reinforced panels dimensions – Vertical stiffeners.

Dimensions – Vertical Stiffeners	
Thickness	6.35 mm
Height	25.4 mm
Width	25.4 mm

Table 5.15- -Reinforced panels dimensions – Upper Horizontal stiffeners.

Dimensions – Upper Horizontal Stiffeners	
Web Thickness	7.94 mm
Height	38.1 mm
Upper Flange Width	58.74 mm
Upper Flange Thickness	7.94 mm

Table 5.16 - Reinforced panels dimensions – Lower Horizontal stiffeners.

Dimensions – Lower Horizontal Stiffeners	
Web Thickness	4.76 mm
Height	29.37 mm
Lower Flange Width	29.37 mm
Lower Flange Thickness	4.76 mm

The results from the two models were compared, the first eigenvalue from the linear buckling analysis, and the load step when the diagonal tension is complete, and the panel's web redistribute the compressive load to the stiffeners from the non-linear analysis. The FEM plots are presented in Figures 5.13 and 5.14, and the comparison in Table 5.17.

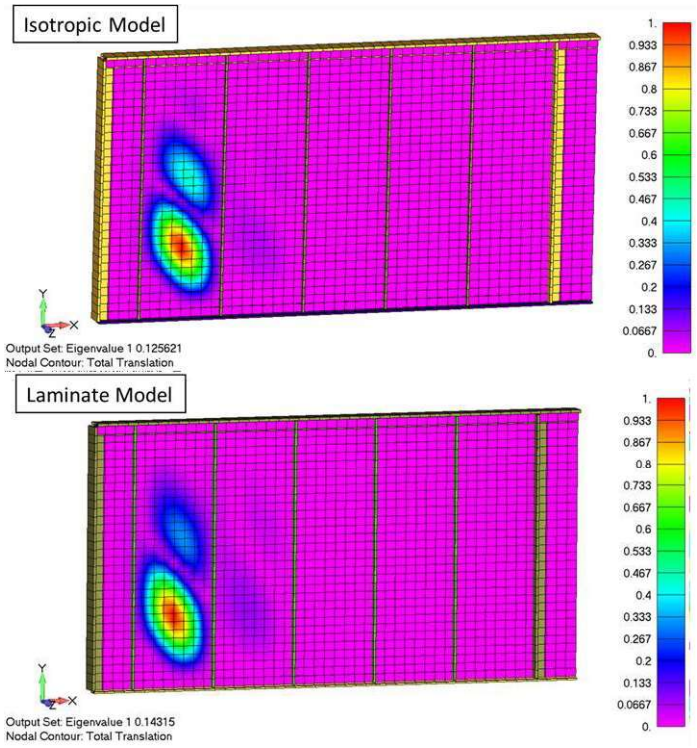

Figure 5.13 - Isotropic and composite models: first eigenvalue (linear buckling analysis) comparison.

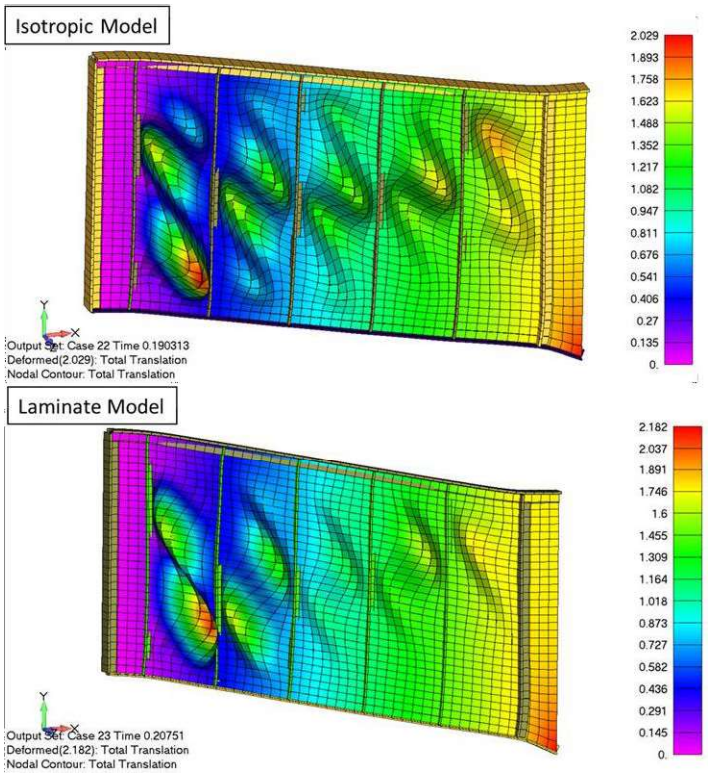

Figure 5.14 - Isotropic and composite models: complete diagonal tension first occurrence (non-linear analysis) comparison (deformations are plotted to scale at 150 times their actual value).

Table 5.17 - Comparison between Isotropic and Composite models.

	First Eigenvalue	**First occurrence of Diagonal Tension**
Isotropic Model	0.125621	0.190313
Composite Model	0.14315	0.20751
Difference	1.75%	1.72%

The results from comparison between Isotropic and Composite models, presented in Table 5.17, show that the greatest difference is 1.75%. These encouraging results create the necessary confidence to use the FEM model in the following analyses.

5.3 Composite Reinforced Panel

Knowing that the FEM can be used to model the composite reinforced panel and to predict the post-buckling behavior, the model was used to choose the best laminate and compared it with the metallic reinforced panel. Six different laminates were selected to be compared, using carbon/epoxy tape (same properties and allowable presented in Tables 5.9 and 5.10), all having 0º, +45º, -45º and 90º, being balanced and symmetric (the reasons for this choices were presented in Section 5.2). It was chosen to use the same material and fiber orientations and just change the stacking sequence because as mention by Kassapoglou, 2013, the buckling modes are more sensitive to this type of variation. All the different stacking sequence are shown in Table 5.18.

Table 5.18 - Selected stacking sequence to be compared.

Model 1	$[0/90/45/-45]_S$
Model 2	$[45/-45/0/90]_S$
Model 3	$[45/0/90/-45]_S$
Model 4	$[0/45/-45/90]_S$
Model 5	$[0/45/90/-45]_S$
Model 6	$[45/0/-45/90]_S$

The reinforced panel dimensions and their vertical and horizontal stiffeners material and dimensions were the same as used in the first composite reinforced panel presented (see Tables 5.12 to 5.16).

For each model it was applied seven loads, in order to verify the laminate behavior with different load magnitudes. For all models, it was evaluated the Laminate Max Failure Index using the Tsai-Wu criterion and Maximum Strain criterion, calculated by the software FEMAP 11.2®. The failure index was used to classify the stress state of the laminate and not to determine the failure of a lamina, therefore the failure indices values presented are not close to one (that indicated failure).

Because of convergence problems in the models, not all the loads used for one criterion could be used for the other. The loads applied in the model for each criterion are presented in Table 5.19.

Table 5.19 - FEM applied loads for each criterion.

	Tsai-Wu	**Maximum Strain**
Condition 1	5500 N	5500 N
Condition 2	100000 N	100000 N
Condition 3	160000 N	160000 N
Condition 4	310000 N	310000 N
Condition 5	500000 N	480000 N
Condition 6	700000 N	700000 N
Condition 7	800000 N	900000 N

The results are presented in Figures 5.15 and 5.16.

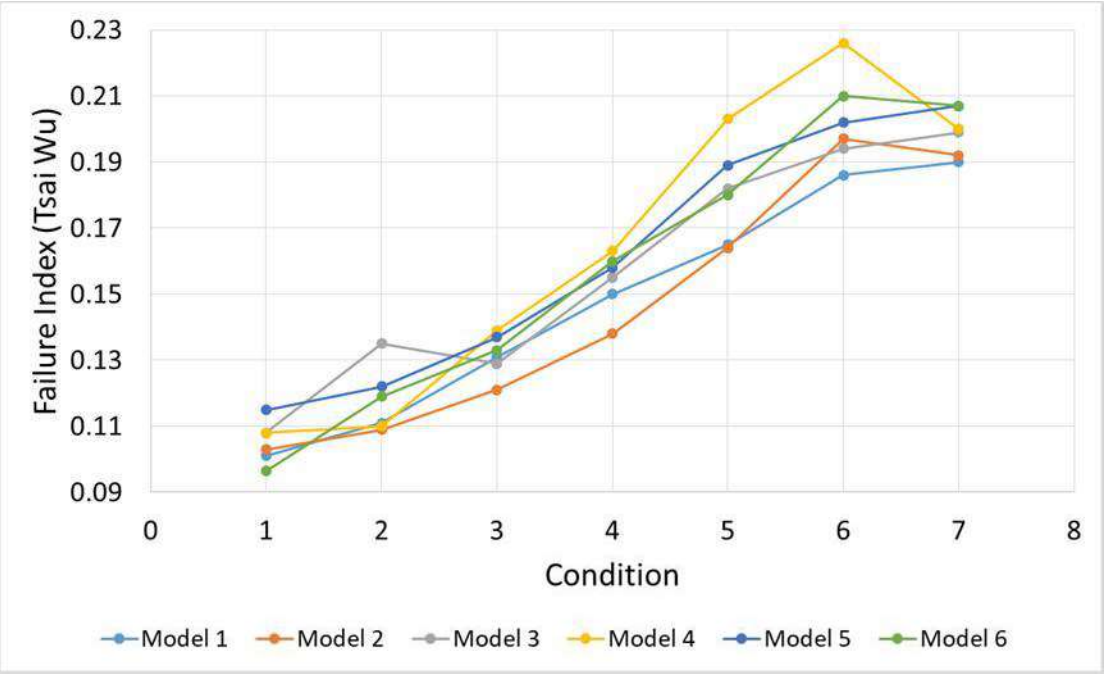

Figure 5.15 - Comparison of the Tsai-Wu Failure Index for all the models.

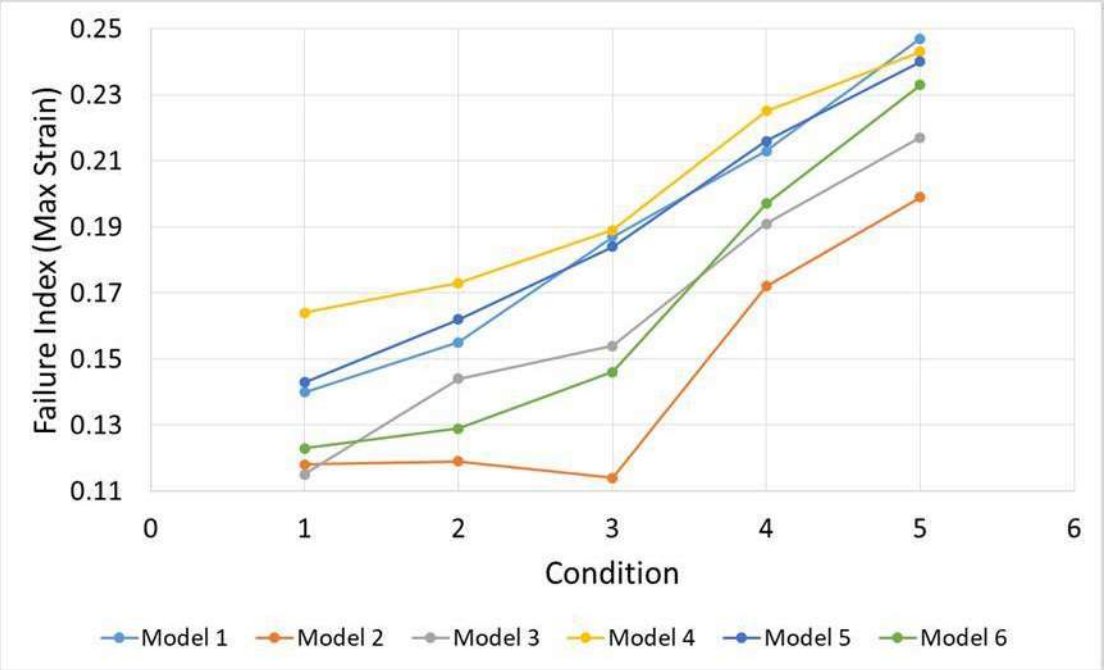

Figure 5.16 - Comparison of the Max Strain Failure Index for all the models.

Analyzing Figures 5.15 and 5.16 it is possible to conclude that the model that have the best behavior in the post-buckling is Model 2, because it presents the lowest failure index for the two criteria compared to all the other models. This result is corroborated by Bailie, Ley and Pasricha, 1997 that affirm for stability is better to use the +45º and -45º plies on the outer surfaces.

5.4 Composite Reinforced Panel versus Metallic Reinforced Panel

In order to verify which reinforced panel, metallic or composite, has the best behavior for the post-buckling analysis, the composite reinforced model chosen before (Model 2) was compared with a metallic reinforced model. Both models had the same mass and a load of 180000 N was applied in both panels.

The two reinforced panels use the same vertical and horizontal stiffeners, the web's thickness was the only parameter changed in the metallic one. Using the Aluminum 2524 T3 and Tape carbon/epoxy (AS4/APC2) densities, it was possible to calculate the web's thickness for the metallic reinforced panel which gives the same weight as the composite reinforced panel. Table 5.20 shows the thickness and mass for the two models.

Table 5.20 - Thickness and mass for the composite and metallic models.

	Composite Reinforced Panel	**Metallic Reinforced Panel**	**Difference**
Web's thickness [mm]	1.520	0.701	-53.87%
Mass [kg]	14.330	14.330	0.00%

The results from the two model were compared, the first eigenvalue from the linear buckling analysis, and the load step when the diagonal tension is complete, and the panel's web redistribute the compressive load to the stiffeners from the non-linear analysis. The FEM plots are presented in Figures 5.17 and 5.18, and the comparison in Table 5.21.

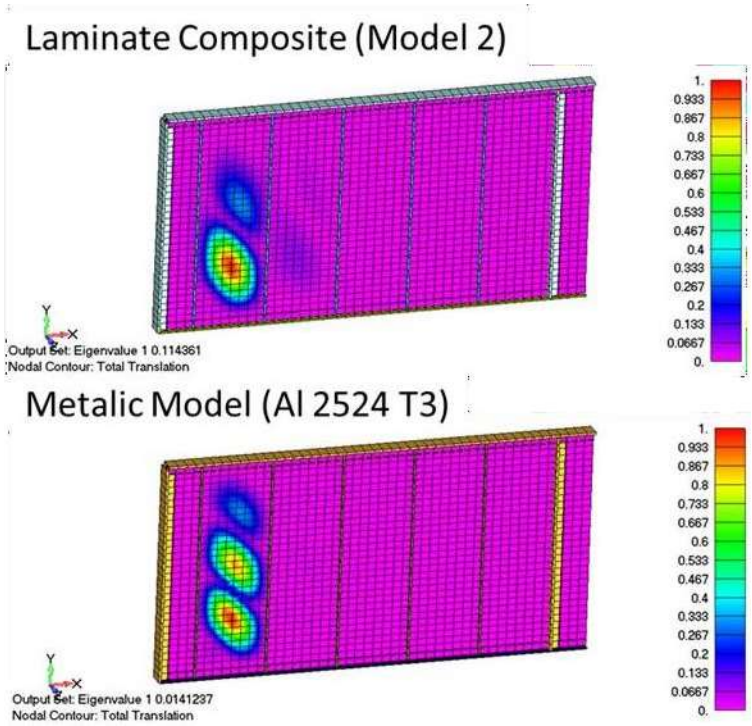

Figure 5.17 - Composite and metallic models: first eigenvalue (linear buckling analysis) comparison.

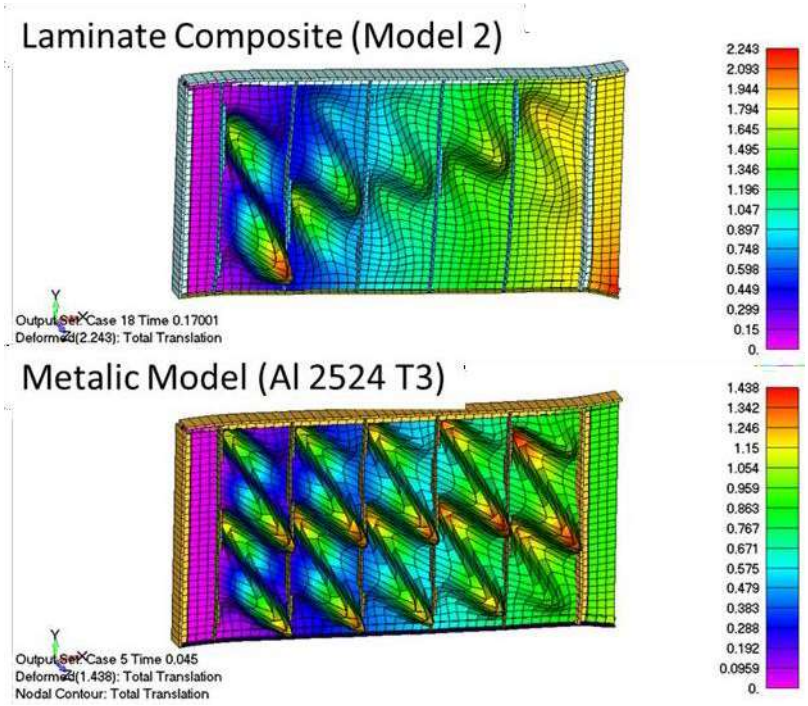

Figure 5.18 - Composite and metallic models: complete diagonal tension first occurrence (non-linear analysis) comparison (deformation scaled in 150 times).

Table 5.21 - Comparison between results from Composite and Metallic models.

	First Eigenvalue	First occurrence of complete Diagonal Tension
Composite Model	0.114361	0.17001
Metallic Model	0.014124	0.04500

The comparison of the results of the two reinforced panels with the same mass, shows that the metallic reinforced panel supports lower loads before the buckling than the composite reinforced panel. This means that the web of the composite reinforced panel withstands to greater loads than the metallic one, consequently redistributes less load for the stiffeners. This result is corroborated by the analyses of Figure 5.19, which shows the comparison of stiffeners axial stress for both of the reinforced panels.

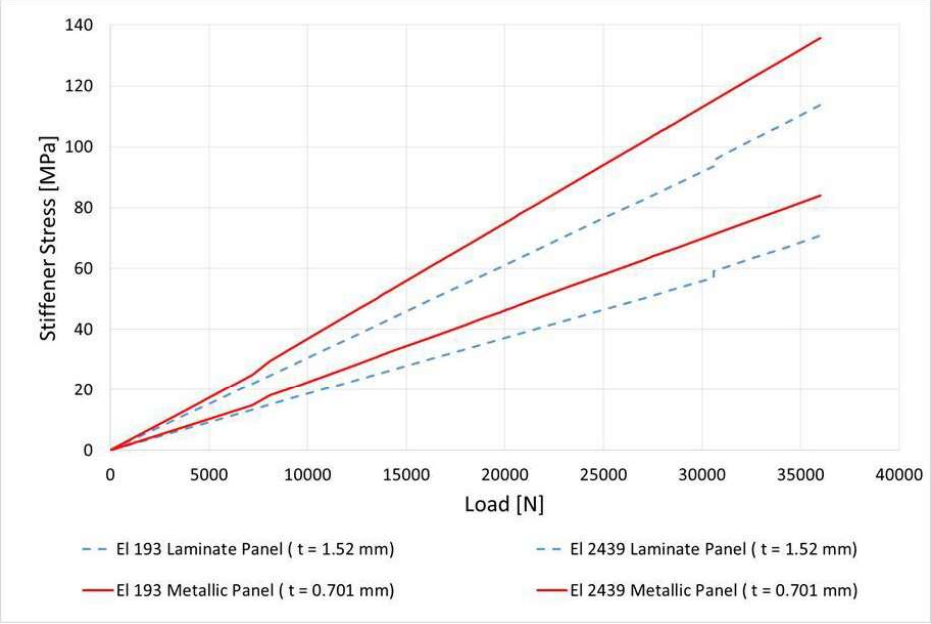

Figure 5.19 - Stress on the stiffener for the composite and metallic models.

Therefore, it is possible to conclude that the composite reinforced panel presents the best behavior for the post-buckling, in the conditions analyzed in this study (FEM boundary conditions, materials, etc).

In order to determine the mass of the metallic reinforced panel for its behavior becomes similar to the composite reinforced panel, a new metallic reinforced panel was built. The web's thickness for the its panel was increased until its first eigenvalue and its load step when the diagonal tension is complete, and the panel's web redistribute the compressive load to the stiffeners got closer to the values for the composite reinforced panel. Table 5.22 shows the thickness and weight for the two models.

Table 5.22 - Thickness and mass for the composite and new metallic models.

	Composite Reinforced Panel	**New Metallic Reinforced Panel**	**Difference**
Web's thickness [mm]	1.52	1.51	-0.82%
Mass [kg]	14.330	17.368	21.20%

The FEM results for the two models are presented in Figures 5.20 and 5.21, and the comparison in shown Table 5.23.

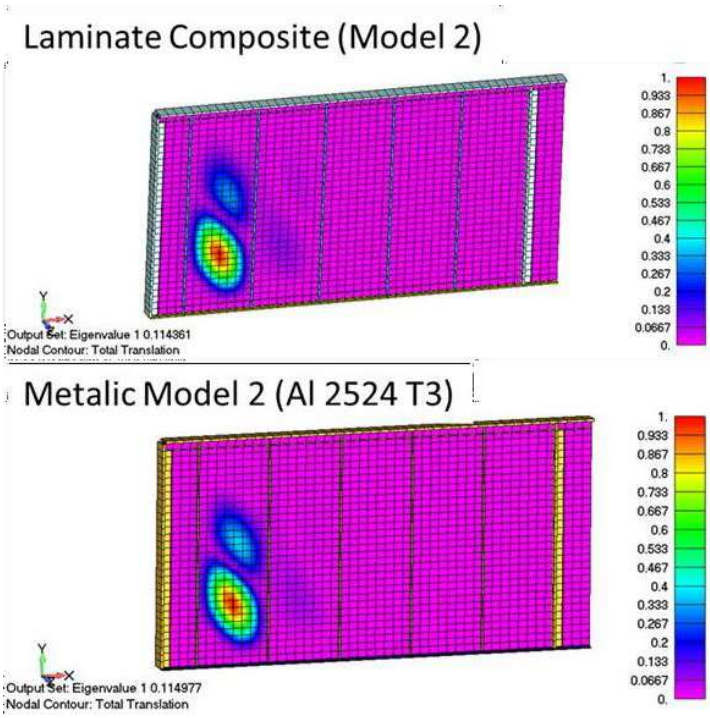

Figure 5.20 - Composite and new metallic models: first eigenvalue (linear buckling analysis) comparison.

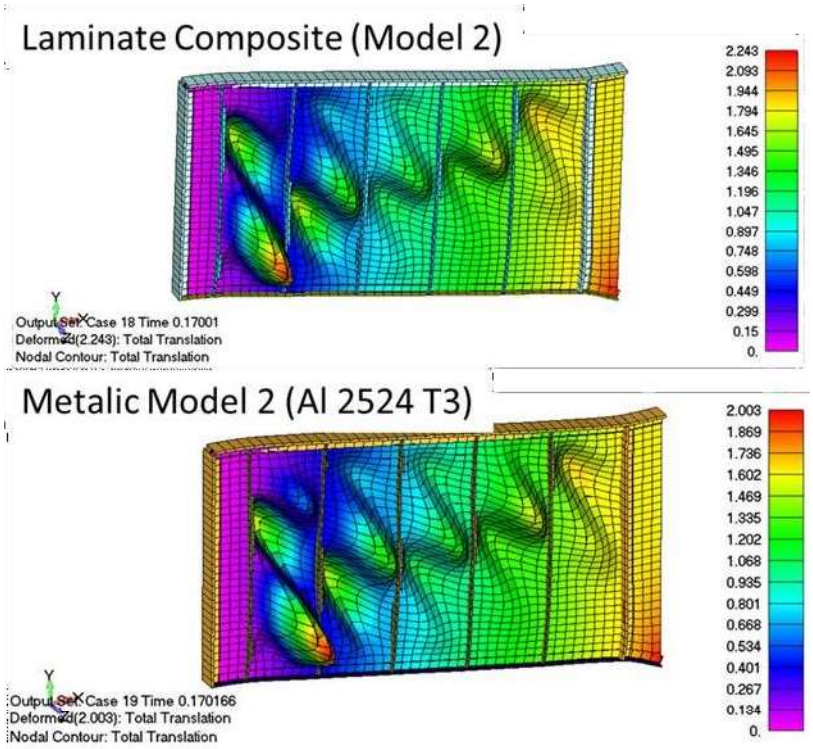

Figure 5.21 - Composite and new metallic models: complete diagonal tension first occurrence (non-linear analysis) comparison (deformation scaled in 150 times).

Table 5.23 - Comparison between composite and new metallic models.

	First Eigenvalue	**First occurrence of complete Diagonal Tension**
Composite Model	0.114361	0.170010
New Metallic Model	0.114977	0.170166

6

6 CONCLUSION

The aim of this study was to improve the understanding of the post-buckling behavior in composite reinforced panels, by verifying the influence of stacking sequence in this performance. Moreover, evaluate if the composite reinforced panel have a better behavior in the post-buckling analysis than the metallic one was also a purposed.

A Literature review revealed that most studies are trying to adapt the method NACA TN2661 (Kuhn, Peterson and Levin, 1952a), used to design metallic reinforced panels, for the composite ones, taking into account the material's anisotropy. But they do not consider the fact that the anisotropy is not the only characteristic of the material that affects the post-buckling behavior. Stacking sequence, and fibers orientation have influence in buckling analysis, therefore they have effects in the post-buckling behavior.

Therefore, the main goals of this study were to develop a method to calibrate a FEM to represents the post-buckling behavior of the composite reinforced panel without having to use experimental results; study the influence of stacking sequence in post-buckling behavior; choose the reinforced panel that have the best behavior during the post-buckling analysis: metallic or composite.

The methodology adopted was to build a FEM for the metallic reinforced panel, and to compare its results with the method NACA TN2661 (Kuhn, Peterson and Levin, 1952a). The model was modified until the differences reached a value smaller than the error previous defined. Using the calibrated model, two FEM were developed for the composite reinforced panel, an isotropic one, using equivalent properties, and the other modeling each layer. The results for both models were compared to verify if the model developed in this study could be used to model a

composite reinforced panel modeling each layer. Then it was compared the failure index for six models of composite reinforced panel, having the same material, but varying the stacking sequence. The one having the lower value of the failure index was considered to have the best post-buckling behavior. This model was then compared with the metallic reinforced panel, having the same mass, in order to verify which panel has the best behavior during the post-buckling event.

The results from this study have shown that it was possible to represent the behavior of the composite reinforced panel during post-buckling using the FEM developed. For this FEM it was modeled each layer of the $[45/-45/0/90]_S$ laminate, which was balanced and symmetric. The boundary conditions and load used were described in section 5, Discussion.

Then six models with different layups were modeled, using the same material, the same total number of layers and the same number of layers for each orientation. The order of the layers was changed to evaluate the influence of the stacking sequence in the post-buckling behavior. Comparing the failure indices for all the models in the moment when the diagonal tension is complete and the panel's web redistribute the compressive load to the stiffeners, it was concluded that the model that has better results, or lower failure index, is the one with +45 and -45 at the outside layers.

Two FEM were built for the metallic and composite reinforced panels, having the same mass, using the same stiffeners, only varying the web thickness. The comparison between buckling analysis and post-buckling behavior shown the composite panel supports more load before the buckling than the metallic one. This means that the web of the composite reinforced panel withstands to greater loads than the metallic one, and consequently redistributes less load for the stiffeners. Therefore, it is possible to conclude that the composite reinforced panel presents the best behavior during the post-buckling event.

6.1 Suggestions for Future Studies

This work has been focused in the analysis of the post-buckling behavior of a panel's web made of carbon/epoxy tape using finite element model. But some other analysis and experiments have been left out, therefore hereafter are presented some suggestions for future work

- Perform tests at composite reinforced panels and compare the results with the one from finite element model, in order to verify if the models could represent the structure post-buckling behavior;
- Test and compare a metallic and a composite reinforced panels in order to verify if the composite has a better behavior for the post-buckling analysis;
- Use a different tape material, other than carbon/epoxy, or a fabric to build the finite element models and execute the same analysis described in this work to verify if the results are the same.
- Change the horizontal and vertical stiffeners material from metal to composite, and perform the same analysis described in this work to verify if the results are the same.

7

7 REFERENCES

AGARWAL, B. L. Post-buckling behavior of composite shear webs. AIAA JOURNAL, Seattle, v. 19, n. 7, p. 933-939, 1981.

ARAKAKI, F. K.; FARIA, A. R. Composite-stiffened panel design under shear post-buckling behavior. Journal of Composite Materials, v. 50, n. 26, p. 3643-3662, 2016.

BAILIE, J. A.; LEY, R. P.; PASRICHA, A. A summary and review of composite laminate design guidelines. Langley RC, Hampton, 1997.

BRAZ, T. B. C. Comportamento em flambagem e pós-flambagem de painel aeronáutico reforçado com laminado de camada fina versus camada grossa. 2018. 49 f. Monografia (graduação em engenharia mecânica) – Escola de engenharia, Universidade Federal de Minas Gerais, Belo Horizonte, 2018.

BRUHN, E. F. Analysis and design of flight vehicle structures. U.S.A.: Tri-State Offset Co., 1973. 996 p.

DANIEL, I. M.; ISHAI, O. Engineering mechanics of composite materials. New York: Oxford university press, 1994. 410 p.

DEGENHARDT, R. et al. Design and analysis of stiffened composite panels including post-buckling and collapse. Computers & Structures, v. 86, n. 9, p. 919-929, 2008.

HERRERO, J. Buckling, post-buckling, and progressive failure analysis of hybrid composite shear webs using a continuum damage mechanism model. 2007. 208 f. Dissertation (Master of Science in mechanical engineer) – Whichita State University, Orone, 2007.

JODOIN, A. et al. Diagonal tension in fibre-metal laminates. In: ICAS 2002, 23, 2002, Toronto. p. 7-8.

KASSAPOGLOU, C. Design and analysis of composite structures: with applications to aerospace structures. Chichester: John Wiley & Sons, 2013. 318 p.

KUHN, P. Stresses in aircraft and shell structures. New York: McGraw-Hill, 1956. 460 p.

KUHN, P; PETERSON, J. P.; LEVIN L. R. A Summary of Diagonal Tension: Part I – Methods of Analysis. NACA Tech. Note 2661: may, 1952a.

KUHN, P.; PETERSON, J. P.; LEVIN L. Ross. A Summary of Diagonal Tension: Part II – Experimental Evidence. NACA Tech. Note 2662: may, 1952b.

MELO, J. D. D. Post-buckling behavior of composite panes in shear. 1993. 95 f. Thesis (PhD) – University of Main, Orone, 1993.

NASTRAN, M. S. C. Quick reference guide. MSC. SOFTWARE, v. 1, 2012a.

NASTRAN, M. S. C. Linear Static Analysis User's Guide. MSC. SOFTWARE, v. 1, 2012b.

NASTRAN, M. S. C. Implicit Nonlinear (SOL 600) User's Guide. MSC. SOFTWARE, v. 1, 2012c.

NETTLES, A. T. Basic mechanics of laminated composite plates. NASA, 1994.

NIU, M. C. Airframe Stress Analysis and Sizing. 2nd ed. Hong Kong: Conmilit Press Ltd., 2005. 810 p.

PEREIRA, D. H. R. Projeto e análise de uma fuselagem flambante sujeita a um campo de tração diagonal. 2017. 109 f. Monografia (graduação em engenharia mecânica) – Escola de engenharia, Universidade Federal de Minas Gerais, Belo Horizonte, 2017.

WAGNER, H. Structures of Thin Sheet Metal: Their Design and Construction. NACA Tech. Memo. 490: December, 1928.

WITTENBERG, T. C.; VAN BATEN, T. J.; DE BOER, A. Design of fiber metal laminate shear panels for ultra-high capacity aircraft. Aircraft Design, v. 4, n. 2-3, p. 99-113, 2001.

8

8 APPENDIX

8.1 Hand Calculation Spreadsheet for method NACA TN2661

Using the software Excel® it was build a spreadsheet to perform the hand calculation for the method NACA TN2661 (Kuhn, Peterson and Levin, 1952a). An image reader software was utilized to transform the graphs presented in NACA method into equation, in order to automate the calculations. The results of these transformations are presented in Figure 3.10 to Figure 3.15 presented in section 3 Bibliography Review. And the Eqs. from (3.4) to (3.8) described in section 3 Bibliography Review were implemented in the spreadsheet. Figure 8.1 shows the sheet "Calculation" from the spreadsheet.

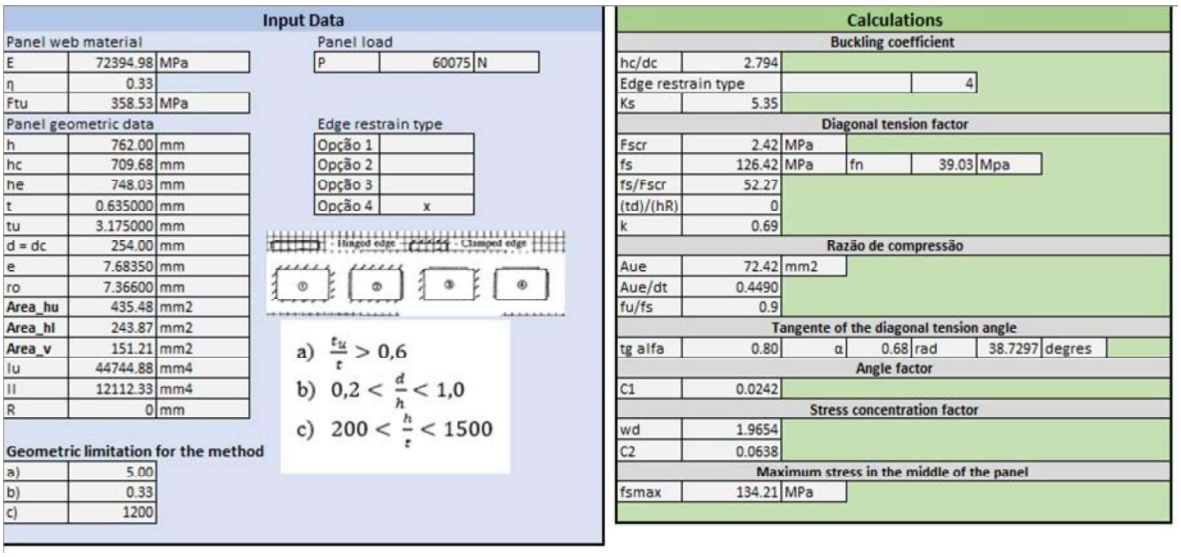

Figure 8.1 – Hand Calculation Spreadsheet: sheet "Calculation".

The user must input data as geometry information, as web's thickness or horizontal stiffener height, material information, as the Young's modulus, and the load applied in the panel at the blue part where it is written "Input Data".

To guarantee that the NACA TN2661 (Kuhn, Peterson and Levin, 1952a) geometric limitations would be respected, it was used the Data Validation from Excel®. With this tool it was created a relation between the geometric variables involved in these limitations, and in case of the violation of the limitation the appearance of an error message. In Figure 8.2 and Figure 8.3 are presented a geometric restriction and an error message, respectively.

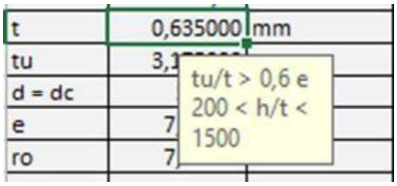

Figure 8.2 – Example of a geometric restriction created with Data Validation tool.

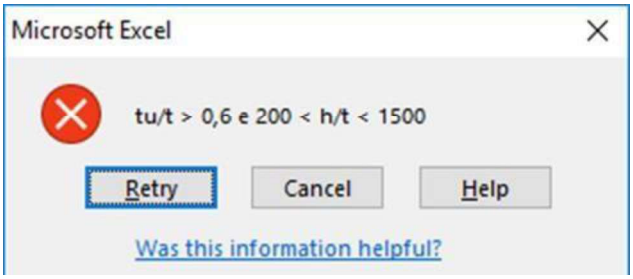

Figure 8.3 – Example of a error message created with Data Validation tool.

An example from Bruhn, 1973 was used to verify if the spreadsheet calculations were correct. The geometry is shown in Figure 8.4, and the comparison between the book's results and the ones calculate with the spreadsheet are presented in

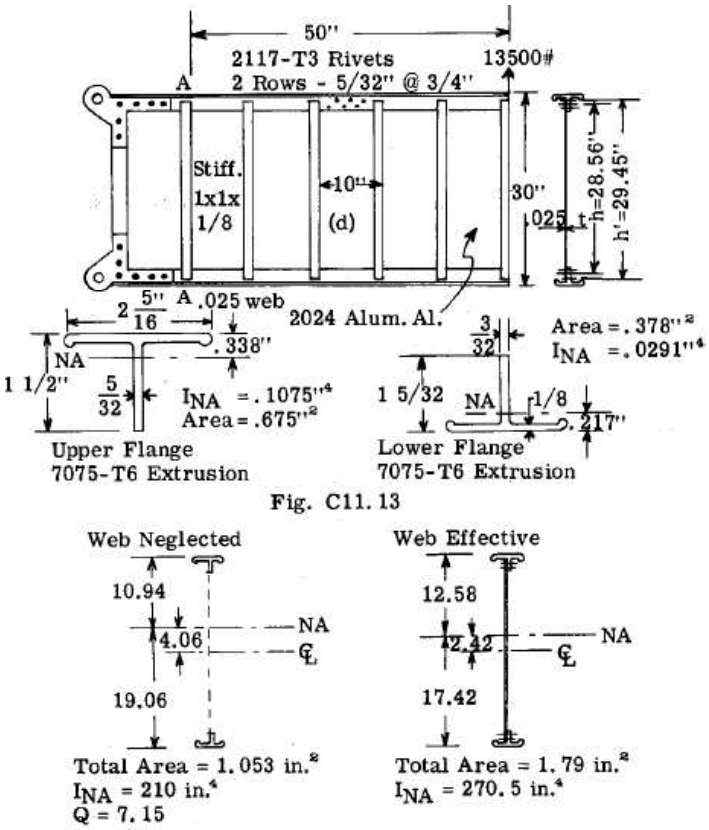

Figure 8.4 – Diagonal tension calculation - Example from Bruhn, 1973.
Bruhn, 1973, p. C 11.10.

Table 8.1 – Results comparison: literature and spreadsheet.

Parameters	Spreadsheet	Calculation at Bruhn, 1973	Difference
Fscr [psi]	350,816	370,00	-5%
Fs [psi]	18336,2	18336,163	0%
k	0,69	0,69	0%
fu/fs	0,90	0,92	-2%
tg α	0,80	0,815	-2%
C1	0,02421	0,022	10%
C2	0,06381	0,075	-15%
wd	1,96539	1,96	0%
fsmax [psi]	19465,5	19577,8	-1%